Constraining mean-field models of the nuclear matter equation of state at low densities

M.D. Voskresenskaya, S. Typel

GSI Helmholtzzentrum für Schwerionenforschung GmbH, Theorie, Planckstraße 1, D-64291 Darmstadt, Germany

Abstract

An extension of the generalized relativistic mean-field (gRMF) model with density dependent couplings is introduced in order to describe thermodynamical properties and the composition of dense nuclear matter for astrophysical applications. Bound states of light nuclei and two-nucleon scattering correlations are considered as explicit degrees of freedom in the thermodynamical potential. They are represented by quasiparticles with medium-dependent properties. The model describes the correct low-density limit given by the virial equation of state (VEoS) and reproduces RMF results around nuclear saturation density where clusters are dissolved. A comparison between the fugacity expansions of the VEoS and the gRMF model provides consistency relations between the quasiparticles properties, the nucleon-nucleon scattering phase shifts and the meson-nucleon couplings of the gRMF model at zero density. Relativistic effects are found to be important at temperatures that are typical in astrophysical applications. Neutron matter and symmetric nuclear matter are studied in detail.

Keywords: mean-field models, nuclear matter, virial equation of state, correlations, cluster formation, cluster dissolution, neutron matter

1. Introduction

Correlations are an essential feature of an interacting many-body system such as nuclear matter. They have an impact on the thermodynamical properties and the composition of the matter since the constituent particles can form new nuclear species as bound states. This aspect is particularly important in the description of matter below nuclear saturation density that is employed in theoretical simulations of astrophysical phenomena such as core-collapse supernovae. There, the knowledge of the equation of state (EoS) of neutron-proton asymmetric matter is required in a wide range of densities and temperatures [1, 2]. The description of dense matter is important for the investigation of various stages in supernova explosions and the structure of neutron stars [3]. It is known to affect the effectiveness of the neutrino reheating of the shock wave [4]. The sensitivity of the collapse dynamics on the properties of matter and the composition in this density regime could strongly influence the structure of the proto-neutron star [5].

Although there are many approaches to describe dense matter, in particular at zero temperature, only few models cover the full parameter space needed in most astrophysical applications. Often, they do not supply sufficient information on the thermodynamical and compositional details. Thus, for many years, a very small number of EoS tables was available which have been used in simulations of dynamical astrophysical processes [6–8]. However, in recent years, the interest in developing EoS has surged and several new EoS tables were provided [9–16]. This development was triggered by the needs of astrophysical modelers, the progress in the theoretical description of nuclear matter and an increase of computational power. Nevertheless, approximations and simplifications are still needed for practical purposes.

There are two major paths to build an EoS of warm and dense nuclear matter for practical applications. One approach starts with an ideal mixture of nucleons and nuclei leading to a nuclear statistical equilibrium (NSE) description [11]. The effect of interactions between all constituents can be incorporated with the help of virial corrections. However, at present, only nucleons and light nuclei are considered in practice in such a virial equation of state (VEoS) [17–19] that provides the correct finite-temperature EoS in the limit of very low densities. The results are model independent since they depend only on experimentally determined data, i.e. binding energies of nuclei and scattering phase shifts. Unfortunately, the application of this approach is limited to rather low densities. The dissolution of nuclei and the transition to

uniform neutron-proton matter with increasing density cannot be described properly. In order to simulate such an effect, the heuristic excluded volume mechanism was employed frequently [11]. A second class of EoS models for astrophysical applications is based on self-consistent mean-field methods with neutrons and protons as fundamental constituents. They are considered as quasiparticles with self-energies that contain the information on the interaction which is usually modeled in an effective way and not taken from a realistic nucleon-nucleon (NN) interaction. These mean-field models, both non-relativistic and relativistic, can be very successful in describing finite nuclei and nuclear matter around saturation density $n_{\rm sat} \approx 0.16$ fm [20–23]. But at low densities $n \ll n_{\rm sat}$ they fail to include correlations properly that give rise to inhomogeneities and the formation of many-body bound states, i.e. nuclei. There were attempts to modify the low-density behavior of mean-field models guided by microscopic calculations, see, e.g., Ref. [24] for the zero temperature case. However, it is still challenging to include the formation of clusters properly. The deficiencies of the various models lead to the strategy of patching up or merging different approaches providing a uniform description of warm dense matter.

A recent publication [25] considered a quantum statistical approach to nuclear matter and devised a generalized relativistic mean-field (gRMF) model, which is an extension of the relativistic mean-field model with density dependent couplings (DD-RMF) from Ref. [26]. The gRMF model includes, besides nucleons, light nuclei (^{2}H $= d$, ^{3}H $= t$, ^{3}He $= h$, ^{4}He $= \alpha$) as hadronic degrees of freedom in the Lagrangian. The dissolution of these clusters is modeled by a medium-dependent shift of their binding energies originating mainly from the action of the Pauli principle. All hadronic constituents of the model can be viewed as quasiparticles that interact via the exchange of effective mesons. The gRMF model achieves bridging the two views on nuclear matter, i.e. a mixture of nucleon and nuclei at low densities and nucleons as quasiparticles moving in mean fields at high densities. Even though the model contains the same relevant particles at low densities as the VEoS, it does not reproduce exactly the thermodynamical properties of the VEoS as will be shown below. In fact, all presently employed EoS for astrophysical applications that are based on mean-field concepts share the problem of reproducing the VEoS in the low-density limit. Thus the question arises, how the models can be modified in order to approach the correct low-density limit. Is a modification of the effective interaction sufficient to meet this aim or are there more severe changes of the models required?

In this work we propose an approach that introduces bound and scattering states in an effective way as additional degrees of freedom in the thermodynamical potential. All relevant quantities are derived in a thermodynamically consistent way. These many-body bound and scattering states are represented by quasiparticles with medium-dependent properties and temperature dependent energies. The low-density behavior of nuclear matter at finite temperatures is considered in detail by comparing the VEoS with the gRMF approach by means of a series expansion of the grand canonical potential in powers of the nucleon fugacities. From the comparison of the VEoS and gRMF expansions we will derive consistency relations that connect quasiparticle properties with the meson-nucleon couplings in the vacuum and the phase shifts or effective-range parameters of nucleon-nucleon scattering. We investigate different choices of the meson-nucleon couplings and quasiparticle properties set by these consistency relations. In addition, relativistic corrections to the traditional VEoS are obtained from these relations that become larger than the effects of particle correlations in the low-density limit. Various parametrizations of the quasiparticle medium dependence are discussed. Studying thermodynamical properties of the matter we consider temperatures higher than the critical temperatures for pairing and Bose condensation in order to avoid these more complex effects. Thus our consideration of the low and zero temperature limits should be corrected in the future to incorporate condensation phenomena. Our approach is not limited to the chosen particular gRMF model with density-dependent meson-nucleon couplings. It can be applied easily to other mean-field approaches as well.

This paper is organized as follows. In Section 2 we present a general formulation of the VEoS that serves as one starting point of the discussion. Basic quantities are defined and the notation is established. We show that correlations in continuum states can be represented effectively by temperature dependent resonances. Analytic expressions for the second virial coefficients are found with the help of the effective-range expansion for the s-wave phase shifts. The connection of the VEoS and NSE models is established. The relation between the VEoS and the generalized Beth-Uhlenbeck approach, which takes into account modifications due to medium effects, is discussed. The gRMF model with density-dependent meson-nucleon couplings is sketched in Section 3 and a series expansion of the grand canonical potential Ω in powers of fugacities is derived for low densities. The power series for Ω in the VEoS and gRMF are compared up to second-order leading

to consistency relations between the models that are studied in various limits. In Sect. 4 we consider an extension of the gRMF model: in order to satisfy consistency relations we introduce temperature dependent resonance energies of the scattering states and modified degeneracy factors that allow to make a smooth interpolation between VEoS and gRMF models. We find that relativistic corrections to the standard VEoS are important in these consistency relations already in the first order of the expansion. The particular example of neutron matter is presented in Section 5 and symmetric nuclear matter is discussed in Section 6. The following section deals with the transition from low to high densities and the occurring problems. Concluding remarks and an outlook are given in Section 8. The comparison of our notations with the ones given in Ref. [18] can be found in Appendix A. An expansion of the energy per particle in neutron matter at zero temperature in powers of the Fermi momentum is considered in Appendix B. Throughout this work we use natural units such that $\hbar = c = 1$.

2. Equation of state in the virial limit

2.1. General formalism

The VEoS represents a model-independent approach in the calculation of thermodynamical properties of low-density matter at finite temperatures T. In the non-relativistic limit, which is usually considered, it describes a system of interacting particles $i, j, \ldots$ with non-relativistic chemical potentials μ_i in a volume V, provided the fugacities $z_i = \exp(\mu_i/T)$ are small ($z_i \ll 1$). The range of densities where the virial expansion is valid can be estimated by the relation $n_i \lambda_i^3 \ll 1$ where n_i is the number density of particle i with mass m_i and $\lambda_i = \sqrt{2\pi/(m_i T)}$ is the thermal wavelength.

The following presentation gives a generalized and more symmetric formulation of the virial approach as compared to [17–19]. The S-matrix formulation by Ref. [27] that was recently applied to nuclear matter in Ref. [28] gives essentially identical results.

Under the presupposed conditions the grand canonical partition function $\mathcal{Q}$ can be expanded in powers of fugacities as

$$\mathcal{Q}(T, V, \mu_i) = 1 + \sum_i Q_i z_i + \frac{1}{2} \sum_{ij} Q_{ij} z_i z_j + \frac{1}{6} \sum_{ijk} Q_{ijk} z_i z_j z_k + \ldots \qquad (1)$$

with one-, two-, three-, ... many-body canonical partition functions Q_i, Q_{ij}, Q_{ijk}, ... In classical non-relativistic mechanics, the single-particle canonical

partition function is

$$Q_i = \frac{g_i}{(2\pi)^3} \int d^3r_i \int d^3p_i \, \exp\left(-\beta H_i\right) = \frac{g_i}{\lambda_i^3} V \tag{2}$$

with the spin degeneracy factor g_i (= 2 for each nucleon), $\beta = 1/T$ and the single-particle Hamiltonian $H_i = p_i^2/(2m_i)$ that only contains a kinetic contribution with momentum p_i. For the two-body canonical partition function we have

$$Q_{ij} = \frac{g_i g_j}{(2\pi)^6} \int d^3r_i \int d^3p_i \int d^3r_j \int d^3p_j \, \exp\left(-\beta H_{ij}\right) \tag{3}$$

with the two-body Hamiltonian $H_{ij} = p_i^2/(2m_i) + p_j^2/(2m_j) + V_{ij}$ that includes a two-body potential V_{ij} responsible for the correlations.

Then, the grand canonical potential

$$\Omega(T, V, \mu_i) = -T \ln \mathcal{Q}(T, V, \mu_i) = -pV \, , \tag{4}$$

that is directly related to the pressure p, can be written in the form

$$\Omega(T, V, \mu_i) = \tag{5}$$
$$-TV \left(\sum_i \frac{b_i}{\lambda_i^3} z_i + \sum_{ij} \frac{b_{ij}}{\lambda_i^{3/2} \lambda_j^{3/2}} z_i z_j + \sum_{ijk} \frac{b_{ijk}}{\lambda_i \lambda_j \lambda_k} z_i z_j z_k + \ldots \right)$$

with the (symmetrized) dimensionless cluster (or virial) coefficients

$$b_i(T) = \frac{\lambda_i^3}{V} Q_i \, , \tag{6}$$

$$b_{ij}(T) = \frac{\lambda_i^{3/2} \lambda_j^{3/2}}{2V} \left(Q_{ij} - Q_i Q_j \right) \, , \tag{7}$$

$$b_{ijk}(T) = \frac{\lambda_i \lambda_j \lambda_k}{6V} \left(Q_{ijk} - Q_i Q_{jk} - Q_j Q_{ik} - Q_k Q_{ij} + 2 Q_i Q_j Q_k \right) \tag{8}$$

that depend on the temperature. Without interaction, the two-, three-, ... many-body partition functions factorize, e.g. $Q_{ij} = Q_i Q_j$, and the second, third, ... cluster coefficients b_{ij}, b_{ijk}, ... vanish.

Individual particle number densities are found from the relation

$$n_i = -\frac{1}{V} \left. \frac{\partial \Omega}{\partial \mu_i} \right|_{T, V, \mu_{j \neq i}} = b_i \frac{z_i}{\lambda_i^3} + 2 \sum_j b_{ij} \frac{z_i z_j}{\lambda_i^{3/2} \lambda_j^{3/2}} + 3 \sum_{jk} b_{ijk} \frac{z_i z_j z_k}{\lambda_i \lambda_j \lambda_k} + \ldots \tag{9}$$

with contributions from free particles (first term in the second equation) and correlated pairs, triples, etc. The entropy is

$$\begin{aligned} S &= -\left.\frac{\partial\Omega}{\partial T}\right|_{V,\mu_i} \qquad (10)\\ &= -\frac{5\Omega}{2T} + V\left(\sum_i \frac{c_i}{\lambda_i^3} z_i + \sum_{ij} \frac{c_{ij}}{\lambda_i^{3/2}\lambda_j^{3/2}} z_i z_j + \sum_{ijk} \frac{c_{ijk}}{\lambda_i\lambda_j\lambda_k} z_i z_j z_k + \ldots\right) \end{aligned}$$

with coefficients

$$c_i = T\frac{db_i}{dT} - \frac{\mu_i}{T}\,, \qquad (11)$$

$$c_{ij} = T\frac{db_{ij}}{dT} - \frac{\mu_i+\mu_j}{T}\,, \qquad (12)$$

$$c_{ijk} = T\frac{db_{ijk}}{dT} - \frac{\mu_i+\mu_j+\mu_k}{T}\,. \qquad (13)$$

Other relevant thermodynamical quantities such as the free energy and the internal energy

$$F = \Omega + V\sum_i \mu_i n_i \qquad (14)$$

and the internal energy

$$E = F + TS \qquad (15)$$

can be obtained immediately.

The formulas given above can be generalized to include four-, five-, ... many-body correlations, but already contributions of the three-body term are hardly ever considered in practice. For a given temperature, two-body correlations will always dominate higher-order correlations when the density decreases. Hence, in the following, we will truncate the expansion at second order in the fugacities of the basic constituents.

The quantum mechanical generalization of the virial expansion up to second order was given by Beth and Uhlenbeck [29, 30]. In classical mechanics the interaction potential between the particles is the relevant quantity that appears in the calculation of the virial coefficients. In quantum mechanics, the Schrödinger equation has to be solved with this potential and the obtained eigenstates comprise bound and scattering states. Integrations over phase space are replaced by sums over all eigenstates of the one- and two-body system and it is obvious that the density of states becomes the relevant

quantity. The result for the first virial coefficient b_i is identical to the classical value (6) in the continuum approximation, corresponding to the replacement of the sum over discrete momentum states by an integral. The second virial coefficient can be expressed as an integral over center-of-mass energies E

$$b_{ij}(T) = \frac{1+\delta_{ij}}{2} \frac{\lambda_i^{3/2}\lambda_j^{3/2}}{\lambda_{ij}^3} \int dE \, \exp\left(-\beta E\right) D_{ij}(E) \pm \delta_{ij} g_i 2^{-5/2} \tag{16}$$

with $\lambda_{ij} = \sqrt{2\pi/[(m_i+m_j)T]}$ and the quantity

$$D_{ij}(E) = \sum_k g_k^{(ij)} \delta(E - E_k^{(ij)}) + \sum_l \frac{g_l^{(ij)}}{\pi} \frac{d\delta_l^{(ij)}}{dE} \tag{17}$$

that measures the difference between the density of states of an interacting and free two-particle system. The last term in equation (16) is a quantum statistical correction with the positive (negative) sign if $i = j$ are identical bosons (fermions).

The first contribution to D_{ij} is a sum over all two-body bound states k of the system ij with degeneracy factors $g_k^{(ij)}$ and energies $E_k^{(ij)} < 0$. The second term takes into account continuum correlations in the two-particle system in all channels l with degeneracy factors $g_l^{(ij)}$ via the energy-dependent scattering phase shifts $\delta_l^{(ij)}$. In general, the index l stands for the total and angular orbital momenta of a particular channel. If the phase shift is dominated by a narrow resonance, it jumps by π in a very small energy interval around the resonance energy and the contribution to the virial coefficient resembles that of a bound state. With experimentally known bound state energies and phase shifts, the second virial coefficient b_{ij} and thus the low-density EoS can be calculated in a model-independent way.

The quantum mechanical generalization of the third virial coefficient was discussed in Ref. [31] but actual calculations turn out to be difficult in practice and, thus, they are not considered here. The derivation of the classical VEoS is based on non-relativistic kinematics. In order to include relativistic effects, at least the relativistic dispersion relation of the particles has to be used. The resulting modifications of the virial coefficients will be discussed when the VEoS is compared to the gRMF approach in Section 3.4.

2.2. Application to nuclear matter with arbitrary neutron to proton ratio

In low-density nuclear matter at not too high temperatures, neutrons and protons are the relevant fundamental constituents. Hence, the grand

canonical potential up to second order in the fugacities becomes

$$\begin{aligned}\Omega(T,V,\mu_n,\mu_p) \qquad (18)\\ = \quad -TV\left(\frac{b_n}{\lambda_n^3}z_n+\frac{b_p}{\lambda_p^3}z_p+\frac{b_{nn}}{\lambda_n^3}z_n^2+\frac{b_{pp}}{\lambda_p^3}z_p^2+2\frac{b_{np}}{\lambda_n^{3/2}\lambda_p^{3/2}}z_nz_p\right)\end{aligned}$$

where the symmetry $b_{np}=b_{pn}$ is used. The Coulomb interaction is usually neglected in the VEoS and b_{pp} is replaced by b_{nn} in (18), cf. Ref. [18]. The second virial coefficient b_{nn} receives contributions only from scattering states. It is convenient to split $b_{np}=b_{np0}+b_{np1}$ into two contributions with total isospin $\mathcal{T}=0$ and $\mathcal{T}=1$. The only bound two-body state in the two-nucleon system, the deuteron, appears in the isospin zero channel with $g_d=3$ and $E_d^{(np)}=-B_d=-2.225$ MeV [32]. According to this observation we can write

$$b_{nn}(T) = \frac{\lambda_n^3}{\lambda_{nn}^3}\sum_l g_l^{(nn)}I_l^{(nn)}-g_n2^{-5/2}\,, \qquad (19)$$

$$b_{pp}(T) = \frac{\lambda_p^3}{\lambda_{pp}^3}\sum_l g_l^{(pp)}I_l^{(pp)}-g_p2^{-5/2}\,, \qquad (20)$$

$$b_{np1}(T) = \frac{1}{2}\frac{\lambda_n^{3/2}\lambda_p^{3/2}}{\lambda_{np}^3}\sum_l g_l^{(np1)}I_l^{(np1)}\,, \qquad (21)$$

$$b_{np0}(T) = \frac{1}{2}\frac{\lambda_n^{3/2}\lambda_p^{3/2}}{\lambda_{np}^3}\left[g_d\exp\left(\frac{B_d}{T}\right)+\sum_l g_l^{(np0)}I_l^{(np0)}\right] \qquad (22)$$

with the virial integral

$$I_l^{(ij)}(T)=\int_0^\infty\frac{dE}{\pi}\,\frac{d\delta_l^{(ij)}}{dE}\exp\left(-\frac{E}{T}\right)\,. \qquad (23)$$

Formally, we can write the sum of the scattering contributions in Eqs. (19)-(22) in the form of a single bound state contribution

$$\sum_l g_l^{(ij)}I_l^{(ij)}=\int_0^\infty\frac{dE}{\pi}\,\frac{d\delta_{ij}}{dE}\exp\left(-\frac{E}{T}\right)=\hat{g}_{ij}\exp\left[-\frac{E_{ij}(T)}{T}\right] \qquad (24)$$

with a temperature dependent effective resonance energy $E_{ij}(T)$ in each ij channel by summing the contributions of all partial waves in an effective total phase shift

$$\delta_{ij}(E)=\sum_l g_l^{(ij)}\delta_l^{(ij)}\,. \qquad (25)$$

The effective degeneracy factor $\hat{g}_{ij} = \pm g_0^{(ij)}$ is chosen such that it is identical to the degeneracy factor in the s-wave. The sign is determined by that of the integral.

In order to illustrate the behavior of the phase shifts and effective resonance energies, neutron-neutron scattering is considered in the following. In this example, the sum of the experimental phase shifts receives contributions only from certain partial waves with total angular momentum J and orbital angular momenta l due to the Pauli principle. Taking into account all possible partial waves with $l = 0$, 1 and 2, i.e. the channels $^1S_0$, $^3P_0$, $^3P_1$, $^3P_2$ and $^1D_2$ in spectroscopic notation $^{2S+1}L_J$, one has

$$\delta_{nn}(E) = \delta_{00}^{(nn)} + \delta_{01}^{(nn)} + 3\delta_{11}^{(nn)} + 5\delta_{21}^{(nn)} + 3\delta_{12}^{(nn)} \tag{26}$$

using double indices Jl in $\delta_{Jl}^{(ij)}$ to indicate the partial wave. In Fig. 1 the effective phase shift for the sum of all partial waves with $l \leq 2$ is depicted in comparison with the pure s-wave phase shift. Since there is no experimental data on the nn phase shifts, we use the np data taken from the Nijmegen partial wave analysis [33] to illustrate the comparison between the experimentally known phase shifts and the results using the effective range approximation. Note, that the laboratory energy $E_{\rm lab} = 2E$ of a neutron scattered on the target at rest is used as the argument. At very low energies, both curves are rapidly rising. At energies above ≈ 10 MeV, contributions of higher partial waves become important.

At low temperatures, the virial integral is dominated by the low-energy phase shifts $\delta_l^{(ij)}$ and only the s-wave contributes significantly due to the large derivative with respect to the energy. The effective-range approximation [34] for the s-wave phase shift

$$k \cot \delta_0^{(ij)} = -\frac{1}{a_{ij}} + \frac{1}{2} r_{ij} k^2 \tag{27}$$

with momentum $k = \sqrt{2\mu_{ij}E}$ and effective mass $\mu_{ij} = m_i m_j/(m_i + m_j)$ can be used to specify the energy dependence of $\delta_0^{(ij)}$ with help of the scattering length a_{ij} and the effective range r_{ij}.

Fig. 1 shows the result for the s-wave phase shift using only the scattering length or both the scattering length and the effective range parameter. The experimental phase shift is nicely reproduced by the effective range expansion at very low energies. The contribution of the k^2 term with r_{ij} is essential to obtain a decrease of the s-wave phase shift at higher energies. In this case,

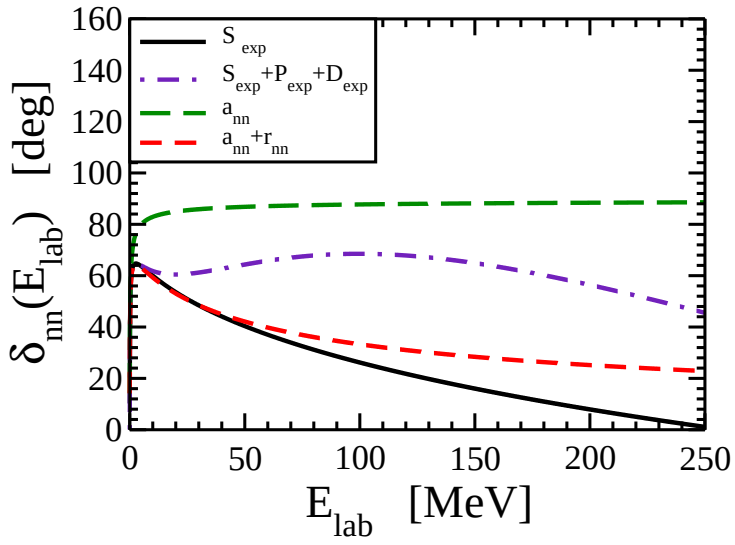

Figure 1: Effective phase shift $\delta_{nn}(E_{\rm lab})$ for neutron-neutron scattering versus laboratory energy $E_{\rm lab} = 2E$. Results are shown using experimental data (including s, p and d-waves or s-waves only) and the effective-range approximation with and without the contribution depending on the effective range parameter, respectively.

the result follows more closely the experimental data, however, differences with respect to the total effective phase shift $\delta_{nn}(E)$ remain.

The effective resonance energy E_{nn} for nn scattering derived from the phase shifts in Eq. (24) is compared for different approximations in Fig. 2. In general, E_{nn} rises smoothly with increasing temperature indicating that it is not dominated by a particular resonance. Contributions of higher partial waves reduce the effective resonance energy as compared to the pure s-wave result.

The s-wave virial integral can be obtained analytically in the effective-range approximation as

$$I_0^{(ij)}(T) \;=\; -\frac{1}{2}\sum_{\eta=\pm 1}\frac{B_{ij}^{(\eta)}}{\sqrt{A_{ij}^{(\eta)}}}\exp\left[\frac{1}{2\mu_{ij}TA_{ij}^{(\eta)}}\right]\mathrm{erfc}\left[\frac{1}{\sqrt{2\mu_{ij}TA_{ij}^{(\eta)}}}\right] \quad (28)$$

for $2r_{ij}/a_{ij} \leq 1$. It depends on the coefficients

$$A_{ij}^{(\eta)} = \frac{a_{ij}^2}{2}\left(1 - \frac{r_{ij}}{a_{ij}} + \eta\sqrt{1 - 2\frac{r_{ij}}{a_{ij}}}\right) \quad (29)$$

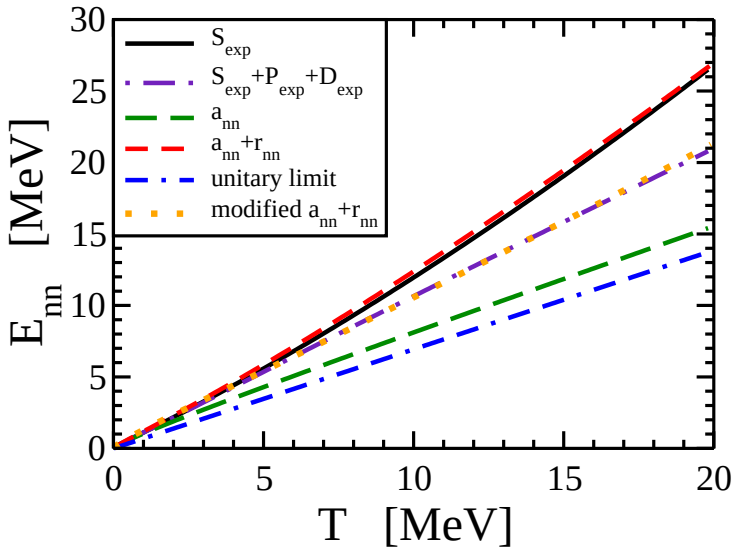

Figure 2: Temperature dependence of the effective resonance energy E_{nn} for neutron-neutron scattering in different approximations. See caption of Figure 1 and text for details.

and

$$B_{ij}^{(\eta)} = \frac{a_{ij}}{2}\left(1+\eta\sqrt{1-2\frac{r_{ij}}{a_{ij}}}\right) . \tag{30}$$

For $r_{ij}=0$ the integral reduces to

$$I_0^{(ij)}(T) \;=\; -\frac{a_{ij}}{2|a_{ij}|}\exp\left(\frac{1}{2\mu_{ij}Ta_{ij}^2}\right)\mathrm{erfc}\left(\frac{1}{\sqrt{2\mu_{ij}Ta_{ij}^2}}\right) . \tag{31}$$

Using these results, the effective resonance energy can be expressed explicitly as a function of the temperature and the effective-range parameters. We use $a_{nn} = -18.818$ fm and $r_{nn} = 2.834$ fm from Ref. [35]. As shown in Figure 2, E_{nn} in the effective range approximation rises more strongly with temperature when the contribution of the r_{nn} term is taken into account. At high temperatures there remains a difference to the exact result that takes higher partial waves into account. However, by a readjustment of the scattering length to $a_{nn} = -11.31$ fm and the effective range to $r_{nn} = 1.06$ fm, the correct effective resonance energy obtained with all partial waves is very well reproduced for the relevant temperatures with the modified parameters

(denoted by modified $a_{nn} + r_{nn}$ in Figure 2). Of course, these modified values for a_{nn} and r_{nn} are not physical and do not describe the scattering in a particular partial wave. They are only an effective means to describe the temperature dependence of the effective resonance energy.

There are several interesting limits for the virial integral. For low temperatures $T \ll A_{ij}^{(\eta)}/(2\mu_{ij})$ one finds

$$I_0^{(ij)}(T) \to -a_{ij}\sqrt{\frac{\mu_{ij}T}{2\pi}} + \dots \tag{32}$$

(independent of the effective range r_{ij}). In the unitary limit $a_{ij} \to -\infty$ and $r_{ij} = 0$, that describes the situation where a bound state/resonance is just at the continuum threshold, $I_0^{(ij)}(T) = 1/2$ and the effective resonance energy is given by $E_{ij} = T \ln 2$. This result is also depicted in Fig. 2. For positive scattering length a_{ij}, e.g. in the deuteron channel, the integral is negative and compensates part of the correlation strength that is located in the bound state of the same channel.

In Ref. [18] also the α-particle was considered as a fundamental constituent in the VEoS and the additional virial coefficients b_α, $b_{n\alpha}$, $b_{p\alpha}$ and $b_{\alpha\alpha}$ appeared in the formalism. (For a comparison of the virial coefficients in the two formulations see Appendix A.) In our approach, the corresponding contributions to Ω represent four-, five- and eight-body correlations that will become irrelevant in the low-density limit as compared to two-nucleon correlations. Since chemical equilibrium requires $\mu_\alpha = 2\mu_n + 2\mu_p + B_\alpha$ with the α-particle binding energy $B_\alpha = 28.296$ MeV [32], the α-particle fugacity $z_\alpha = \exp(\mu_\alpha/T)$ is not independent of the neutron and proton fugacities. The VEoS with neutrons, protons and α-particles was further extended in Ref. [19] to include ^{3}H and ^{3}He as constituent particles corresponding to three-body correlations. Care has to be taken in order to avoid a double counting of states since, e.g., the α-particle states can be obtained in the ^{3}H-p and ^{3}He-n channels (or the neglected ^{2}H-^{2}H channels) that all represent four-body correlations when nucleons are assumed to be the only fundamental particles.

2.3. Relation to the nuclear statistical equilibrium approach

In principle, the virial expansion could be extended to third, fourth, ... order to include more and more many-body correlations. The second, third, ... virial coefficients will contain bound state contributions that cor-

respond to ground and excited states of heavy nuclei. Neglecting the many-body continuum correlations, the grand canonical potential becomes a sum

$$\Omega = -TV \sum_{(A,Z)} \frac{g_{A,Z}}{\lambda_{A,Z}^3} \exp\left(\frac{\mu_{A,Z}}{T}\right) \tag{33}$$

over all nuclei with mass number A, charge number Z, chemical potential $\mu_{A,Z} = (A-Z)\mu_n + Z\mu_p$ and thermal wavelength $\lambda_{A,Z} = \sqrt{2\pi/(m_{A,Z}T)}$. The effective degeneracy factor

$$g_{A,Z}(T) = g_{A,Z}^{(0)} + \sum_k g_{A,Z}^{(k)} \exp\left(-\frac{E_k}{T}\right) \tag{34}$$

is a sum over the ground state 0 and all excited states k of the nucleus ${}^A\mathrm{Z}$ with excitation energies E_k, total angular momenta J_k and $g_{A,Z}^{(k)} = (2J_k+1)$. The summation over individual states is often replaced by an integral over energy with an appropriate level density, see, e.g. Ref. [11]. The temperature dependence of the degeneracy factor is a simple and efficient means to include excited states of nuclei. It will be used below in the formulation of the gRMF approach.

2.4. Generalized Beth-Uhlenbeck approach

The description of matter in the conventional VEoS is limited to rather low densities. However, the approach can be generalized in order to reach higher densities and to include the effects of dissolution of composite particles, i.e. the Mott effect. This generalized Beth-Uhlenbeck (gBU) approach is based on a quantum statistical description with thermodynamic Greens functions. For details see Ref. [36]. The grand canonical potential Ω in the gBU approach assumes a similar form as in the VEoS. The constituents are considered as quasiparticles with the correct statistics (Fermi-Dirac or Bose-Einstein) and with self-energies that contain already some effect of the mutual interaction. The remaining two-body correlations (between quasiparticles!) are contained in a modified second virial coefficient that is given by

$$b_{ij}(T) = \frac{1+\delta_{ij}}{2} \lambda_i^{3/2} \lambda_j^{3/2} \int dE\, f_{ij}(E + E_{\mathrm{cont}}) F_{ij}(E) \tag{35}$$

with the correct distribution function $f_{ij}(E)$ of the composite system, i.e. Bose-Einstein for the two-nucleon-states, and the quantity

$$F_{ij}(E) = \sum_k g_k^{(ij)} \int_{P>P_{\rm Mott}} \frac{d^3P}{(2\pi)^3}\, \delta(E - E_k^{(ij)}) + \sum_l \frac{g_l^{(ij)}}{\pi} \int \frac{d^3P}{(2\pi)^3}\, 2\sin^2\delta_l^{(ij)} \frac{d\delta_l^{(ij)}}{dE} \tag{36}$$

that is related to the in-medium density of states. The main differences as compared to Eqs. (16) and (17) are caused by medium effects. The properties of a two-body system ij depend on the total c.m. momentum $\vec{P}$ of the state with respect to the medium. Hence, there is an additional summation (integration) over $\vec{P}$. Bound states only appear for P larger than the Mott momentum $P_{\rm Mott}$ because at lower total momenta their formation is suppressed by the action of the Pauli principle. The phase shifts $\delta_l^{(ij)}(P, T, \mu_i, \mu_j)$ are determined by the in-medium T-matrix describing the scattering of two quasiparticles. Similarly $E_k^{(ij)}(P, T, \mu_i, \mu_j)$ is the medium-dependent energy of a bound state. Energies in Eq. (36) are measured with respect to the continuum edge $E_{\rm cont}$ that corresponds to the energy in the frame of the medium where the relative momentum of the scattering particles is zero. The $2\sin^2\delta_l^{(ij)}$ factor takes into account that part of interaction effects is already contained in the self-energies of the quasiparticles. The second term in Eq. (36) is related to the number of correlated quasiparticles that is different to the number of correlated particles as calculated by the usual Beth-Uhlenbeck approach in Eq. (17).

3. Generalized relativistic mean-field model

3.1. General formalism

In Ref. [25] a RMF model with density-dependent meson-nucleon couplings was generalized to include light clusters (bound states of ^{2}H, ^{3}H, ^{3}He, ^{4}He) as additional degrees of freedom with medium-dependent binding energies. These clusters couple minimally to the meson fields with a strength that was assumed to be a multiple of the nucleon coupling strength. Scattering states were not considered in the RMF model of in Ref. [25]. The approach can easily be extended when more than the above mentioned nuclei need to be included. Such a model with nuclei as explicit degrees of freedom we call the gRMF model in this paper.

The grand canonical potential of the model can be formulated as a function $\Omega(T, V, \tilde{\mu}_i, \omega, \rho, \sigma, \delta)$ depending on the temperature T, volume V, relativistic chemical potentials $\tilde{\mu}_i = m_i + \mu_i$ of the particles and the spatially constant meson fields ω, ρ, σ and δ under consideration. Here, all four mesons are included to cover the four possible combinations of scalars and vectors in Lorentz and isospin space. We neglect antiparticles in the following because they give sizable contributions only at temperatures much higher than those relevant in the considered astrophysical applications. In the general case of inhomogeneous matter, not discussed here, Ω becomes a functional of the spatially varying meson fields and their gradients.

For uniform nuclear matter, the grand canonical potential can be written as

$$\begin{aligned} \Omega &= \sum_i \Omega_i - V \left[\frac{1}{2} \left(m_\omega^2 \omega^2 + m_\rho^2 \rho^2 - m_\sigma^2 \sigma^2 - m_\delta^2 \delta^2 \right) \right. \\ &\quad \left. + \left(\Gamma'_\omega \omega n_\omega + \Gamma'_\rho \rho n_\rho - \Gamma'_\sigma \sigma n_\sigma - \Gamma'_\delta \delta n_\delta \right) (n_n + n_p) \right] \end{aligned} \tag{37}$$

where Γ'_i are the derivatives of the density dependent couplings which determine the nucleon-meson coupling strength. Contributions from individual particles (nucleons and clusters) are

$$\Omega_i = \mp g_i V T \int \frac{d^3k}{(2\pi)^3} \ln \left[1 \pm \exp \left(-\frac{E_i - \tilde{\mu}_i}{T} \right) \right] \tag{38}$$

where the upper (lower) signs refer to fermions (bosons). In the case of Maxwell-Boltzmann statistics, Eq. (38) reduces to

$$\Omega_i = g_i V T \int \frac{d^3k}{(2\pi)^3} \exp \left(-\frac{E_i - \tilde{\mu}_i}{T} \right) . \tag{39}$$

We assume that the degeneracy factors g_i can depend in general on the temperature as in the case of NSE models, cf. Section 2.3. The densities n_ω, n_ρ, n_σ and n_δ appearing in (37) are themselves functions of the temperature, chemical potentials and meson fields (see below).

The mass of a cluster $i = d, t, h, \alpha, \ldots$ with N_i neutrons and Z_i protons is written as

$$m_i = N_i m_n + Z_i m_p - (1 - \delta_{in})(1 - \delta_{ip}) B_i^{(\mathrm{vac})} \tag{40}$$

with neutron and proton rest masses m_n and m_p, respectively, and the vacuum binding energy $B_i^{(\mathrm{vac})} > 0$ for composite particles. For neutrons and

protons the binding energy does not appear. Chemical equilibrium leads to the constraint

$$\tilde{\mu}_i = N_i \tilde{\mu}_n + Z_i \tilde{\mu}_p \tag{41}$$

for the relativistic chemical potentials of the clusters. With every particle $i = n, p, d, t, h, \alpha, \ldots$ of momentum $\vec{k}$, an energy

$$E_i(\vec{k}) = V_i + \sqrt{k^2 + (m_i - S_i)^2} \tag{42}$$

is associated that contains the vector and scalar self-energies V_i and S_i, respectively. These potentials are given by

$$V_i = \Gamma_{i\omega}\omega + \Gamma_{i\rho}\rho + (\delta_{in} + \delta_{ip})V^{(r)} , \tag{43}$$

$$S_i = \Gamma_{i\sigma}\sigma + \Gamma_{i\delta}\delta - (1 - \delta_{in})(1 - \delta_{ip})\Delta B_i \tag{44}$$

with meson fields $m = \omega, \rho, \sigma, \delta$ and their couplings Γ_{im} to the particle i. We assume that the coupling strength of the clusters is a multiple of that of the nucleons, i.e.

$$\Gamma_{im} = g_{im}\Gamma_m(\varrho) \tag{45}$$

with

$$g_{i\omega} = g_{i\sigma} = N_i + Z_i , \tag{46}$$

$$g_{i\rho} = g_{i\delta} = N_i - Z_i . \tag{47}$$

Other choices are possible and should be explored in the future. The meson-nucleon couplings $\Gamma_m(\varrho)$ depend on the total nucleon density $\varrho = n_n + n_p$ only. The functional form and the parameters of the density dependent couplings $\Gamma_m(\varrho)$ used in the gRMF model were chosen in such a way to describe the properties of finite nuclei and nuclear matter parameters at saturation density. The vector self-energy contains the rearrangement term

$$V^{(r)} = \Gamma'_\omega n_\omega \omega + \Gamma'_\rho n_\rho \rho - \Gamma'_\sigma n_\sigma \sigma - \Gamma'_\delta n_\delta \delta \tag{48}$$

that is only relevant for nucleons. In the medium, the actual binding energy of a cluster $B_i = B_i^{(\mathrm{vac})} - \Delta B_i$ will be shifted with respect to the vacuum value $B_i^{(\mathrm{vac})}$ by a quantity ΔB_i. This medium-dependent binding energy shift ΔB_i for composite particles is parametrized as a function of temperature and the Lorentz vector meson fields ω and σ, see, e.g. Ref. [25]. The specific form of these shifts is not important in the present discussion of the low-density

behavior of the EoS but it affects the transition to high densities, see Section 7.

The source densities in Eqs. (37) and (48)

$$n_\omega = \sum_i g_{i\omega} n_i \,, \quad n_\rho = \sum_i g_{i\rho} n_i \,, \tag{49}$$

$$n_\sigma = \sum_i g_{i\sigma} n_i^{(s)} \,, \quad n_\delta = \sum_i g_{i\delta} n_i^{(s)} \tag{50}$$

depend on the vector and scalar particle number densities n_i and $n_i^{(s)}$, respectively, that are defined as

$$n_i = -\left.\frac{\partial \Omega}{\partial \tilde{\mu}_i}\right|_{T,V,\tilde{\mu}_{j\neq i}} = g_i \int \frac{d^3k}{(2\pi)^3}\, f_i \,, \tag{51}$$

$$n_i^{(s)} = g_i \int \frac{d^3k}{(2\pi)^3}\, f_i \frac{m_i - S_i}{\sqrt{k^2 - (m_i - S_i)^2}} \tag{52}$$

with the Fermi-Dirac (Bose-Einstein) distribution function

$$f_i(\vec{k}) = \left[\exp\left(\frac{E_i - \tilde{\mu}_i}{T}\right) \pm 1\right]^{-1} \tag{53}$$

or the Maxwell-Boltzmann distribution function

$$f_i(\vec{k}) = \exp\left(-\frac{E_i - \tilde{\mu}_i}{T}\right) \tag{54}$$

depending on the particle statistics.

The field equations for the mesons are found from the functional Ω with the help of the Euler-Lagrange equations. They have the form

$$m_\omega^2 \omega = \Gamma_\omega n_\omega + \sum_i (1 - \delta_{in})(1 - \delta_{ip}) n_i^{(s)} \frac{\partial \Delta B_i}{\partial \omega} \,, \tag{55}$$

$$m_\rho^2 \rho = \Gamma_\rho n_\rho + \sum_i (1 - \delta_{in})(1 - \delta_{ip}) n_i^{(s)} \frac{\partial \Delta B_i}{\partial \rho} \,, \tag{56}$$

$$m_\sigma^2 \sigma = \Gamma_\sigma n_\sigma \,, \tag{57}$$

$$m_\delta^2 \delta = \Gamma_\delta n_\delta \tag{58}$$

with additional contributions to the source terms due to the dependence of the binding energies B_i on the vector meson fields. Finally, the entropy is obtained as

$$\begin{aligned} S &= -V\sum_i g_i \int \frac{d^3k}{(2\pi)^3}\,\left[f_i \ln f_i \pm (1\mp f_i)\ln(1\mp f_i)\right] \\ &\quad -V\sum_i (1-\delta_{in})(1-\delta_{ip})\, n_i^{(s)} \frac{\partial \Delta B_i}{\partial T} - \sum_i \frac{\Omega_i}{g_i}\frac{dg_i}{dT} \end{aligned} \tag{59}$$

with the usual single-particle contribution, a term due to the temperature dependence of the cluster binding energy shifts ΔB_i and a contribution caused by internal excitations of the clusters, i.e. the introduction of the temperature dependence of the degeneracy factors, described in Sect. 4. In case of the Maxwell-Boltzmann statistics for a particle i, the integrand contains only the term $f_i \ln f_i$.

3.2. Scheme of the fugacity expansion

Introducing the modified fugacity

$$\tilde{z}_i = \exp\left(\frac{\tilde{\mu}_i - m_i + S_i - V_i}{T}\right) = \exp\left(\frac{S_i - V_i}{T}\right) z_i \tag{60}$$

we write the distribution function as

$$f_i = \left[\tilde{z}_i^{-1}\exp\left(\frac{e_i}{T}\right) \pm 1\right]^{-1} = \frac{\tilde{z}_i \exp\left(-\frac{e_i}{T}\right)}{1 \pm \tilde{z}_i \exp\left(-\frac{e_i}{T}\right)} \tag{61}$$

with the kinetic energy $e_i(k) = \sqrt{k^2 + (m_i - S_i)^2} - (m_i - S_i) \geq 0$. For $\tilde{z}_i \ll 1$ the distribution function can be expanded in a power series in $\tilde{z}_i \exp(-e_i/T)$. The appearing momentum space integrals can be evaluated explicitly [37] with the integral representation of the modified Bessel functions $K_\nu(x)$ [38]. For the contributions (38) of the individual particles to the grand canonical potential we find

$$\begin{aligned} \Omega_i &= -VT\frac{g_i}{\lambda_i^3}\left(\frac{m_i - S_i}{m_i}\right)^{3/2} \\ &\quad \times \sum_{n=0}^{\infty} \frac{(\mp 1)^n}{(n+1)^{5/2}} k_2\left[(n+1)\frac{m_i - S_i}{T}\right] \exp\left[(n+1)\frac{S_i - V_i}{T}\right] z_i^{n+1} \end{aligned} \tag{62}$$

with the non-relativistic fugacity z_i and the functions

$$k_\nu(x) = \sqrt{\frac{2x}{\pi}} \exp(x) K_\nu(x) \,. \tag{63}$$

Similarly, the vector density is obtained as

$$\begin{aligned} n_i = {} & \frac{g_i}{\lambda_i^3} \left(\frac{m_i - S_i}{m_i} \right)^{3/2} \\ & \times \sum_{n=0}^{\infty} \frac{(\mp 1)^n}{(n+1)^{3/2}} k_2 \left[(n+1) \frac{m_i - S_i}{T} \right] \exp \left[(n+1) \frac{S_i - V_i}{T} \right] z_i^{n+1} \,. \end{aligned} \tag{64}$$

For the scalar density $n_i^{(s)}$, k_2 has to be replaced with k_1. In case of Maxwell-Boltzmann statistics, only the $n = 0$ term remains. Without interaction, i.e. $S_i = V_i = 0$, the results for a relativistic Fermi or Bose gas are recovered. For $T \to 0$, i.e. $x = (n+1)(m_i - S_i)/T \to \infty$, one finds from the asymptotic expansion [38]

$$k_\nu(x) = 1 + \frac{\mu - 1}{8x} + \frac{(\mu - 1)(\mu - 9)}{2!(8x)^2} + \frac{(\mu - 1)(\mu - 9)(\mu - 25)}{3!(8x)^3} + \ldots \tag{65}$$

with $\mu = 4\nu^2$ the common expressions

$$\Omega_i = -VT \frac{g_i}{\lambda_i^3} \sum_{m=0}^{\infty} \frac{(\mp 1)^m}{(j+1)^{5/2}} z_m^{m+1} \,, \tag{66}$$

and

$$n_i = \frac{g_i}{\lambda_i^3} \sum_{m=0}^{\infty} \frac{(\mp 1)^m}{(m+1)^{3/2}} z_m^{m+1} \tag{67}$$

for non-relativistic particles. In this limit, $n_i^{(s)} = n_i$, because the scalar density differs from the baryon density only in the relativistic description. Since the scalar and vector self-energies are themselves functions of the densities, a second expansion of the series (62) and (64) is required.

3.3. Fugacity expansion of the grand canonical potential up to second order

In order to compare the true series expansion of the grand canonical potential Ω of the gRMF model with the form (18) in the VEoS approach at low densities, we expand (37) up to second order in the fugacities of neutrons

and protons. In the following we will only consider neutrons, protons and deuterons in the density expansion. Nuclei with mass numbers $A \geq 3$ do not contribute in the second order of expansion since we only consider nucleons as basic constituents. The explicit contribution of the deuteron ground state appears in the two-nucleon correlation term with

$$z_d = z_n z_p \exp\left(\frac{B_d}{T}\right) . \tag{68}$$

For sufficiently low nucleon densities, the self-energies of the nucleons are approximately linear in the nucleon densities. Hence, the contribution of the individual nucleon can be approximated as

$$\begin{aligned} \Omega_i \;\approx\; & -VT\frac{g_i}{\lambda_i^3}\left\{k_2\left(\frac{m_i}{T}\right)\left[1+\frac{S_i}{T}\left(1-\frac{k_2'\left(\frac{m_i}{T}\right)}{k_2\left(\frac{m_i}{T}\right)}-\frac{3}{2}\frac{T}{m_i}\right)-\frac{V_i}{T}\right]z_i \right. \\ & \left. -\frac{1}{2^{5/2}}k_2\left(2\frac{m_i}{T}\right)z_i^2\right\} . \end{aligned} \tag{69}$$

Applying the recursion relation

$$k_\nu'(x) = \left(1-\frac{2\nu-1}{2x}\right)k_\nu - k_{\nu-1}(x) , \tag{70}$$

the expression (69) for the nucleons reduces to

$$\Omega_i \;\approx\; -VT\left[\left(1-\frac{V_i}{T}\right)x_i + \frac{S_i}{T}y_i - \frac{g_i}{2^{5/2}\lambda_i^3}k_2\left(2\frac{m_i}{T}\right)z_i^2\right] \tag{71}$$

with the abbreviations

$$x_i \;=\; \frac{g_i}{\lambda_i^3}k_2\left(\frac{m_i}{T}\right)z_i , \tag{72}$$

$$y_i \;=\; \frac{g_i}{\lambda_i^3}k_1\left(\frac{m_i}{T}\right)z_i . \tag{73}$$

For the deuteron contribution we have

$$\Omega_d \;=\; -VT\frac{g_d}{\lambda_d^3}k_2\left(\frac{m_d}{T}\right)z_n z_p \exp\left(\frac{B_d}{T}\right) \tag{74}$$

without self-energy terms which contribute only in higher order of the fugacities. Contrary the nucleon self-energies contribute already in the lowest order of the fugacities

$$\begin{aligned} V_n &\approx C_\omega(x_n + x_p) + C_\rho(x_n - x_p), && (75)\\ V_p &\approx C_\omega(x_n + x_p) - C_\rho(x_n - x_p), && (76)\\ S_n &\approx C_\sigma(y_n + y_p) + C_\delta(y_n - y_p), && (77)\\ S_p &\approx C_\sigma(y_n + y_p) - C_\delta(y_n - y_p) && (78) \end{aligned}$$

with coefficients

$$C_m = \frac{\Gamma_m^2(0)}{m_m^2} \tag{79}$$

for $m = \omega, \rho, \sigma, \delta$ that depend on the density dependent meson couplings $\Gamma_m(\varrho)$ taken in the limit $\varrho \to 0$. The rearrangement term in the vector self-energy does not contribute at this level because it is at least quadratic in the densities. With the help of the field equations (55)-(58), the mesonic contributions in (37) can be expressed as quadratic forms of the nucleon densities. Finally, after performing all necessary expansions up to second order in the nucleon fugacities, we obtain the resulting grand canonical potential

$$\begin{aligned} &\Omega(T, V, \mu_n, \mu_p) = && (80)\\ &\quad -TV\frac{g_n}{\lambda_n^3}\left[k_2\left(\frac{m_n}{T}\right) z_n - \frac{1}{2^{5/2}} k_2\left(2\frac{m_n}{T}\right) z_n^2\right]\\ &\quad -TV\frac{g_p}{\lambda_p^3}\left[k_2\left(\frac{m_p}{T}\right) z_p - \frac{1}{2^{5/2}} k_2^2\left(2\frac{m_p}{T}\right) z_p^2\right]\\ &\quad -TV\frac{g_d}{\lambda_d^3} k_2\left(\frac{m_d}{T}\right) \exp\left(\frac{B_d}{T}\right) z_n z_p\\ &\quad +\frac{V}{2}\frac{g_n^2}{\lambda_n^6}\left[(C_\omega + C_\rho)\, k_2^2\left(\frac{m_n}{T}\right) - (C_\sigma + C_\delta)\, k_1^2\left(\frac{m_n}{T}\right)\right] z_n^2\\ &\quad +\frac{V}{2}\frac{g_p^2}{\lambda_p^6}\left[(C_\omega + C_\rho)\, k_2^2\left(\frac{m_p}{T}\right) - (C_\sigma + C_\delta)\, k_1^2\left(\frac{m_p}{T}\right)\right] z_p^2\\ &\quad +V\frac{g_n g_p}{\lambda_n^3 \lambda_p^3}\left[(C_\omega - C_\rho)\, k_2\left(\frac{m_n}{T}\right) k_2\left(\frac{m_p}{T}\right)\right.\\ &\quad \left. -(C_\sigma - C_\delta)\, k_1\left(\frac{m_n}{T}\right) k_1\left(\frac{m_p}{T}\right)\right] z_n z_p \end{aligned}$$

with contributions from free nucleons and their correlation due to statistics, the deuteron bound state and the interaction.

3.4. Comparison of fugacity expansions

A comparison of Eq. (18) with the corresponding expansion (80) permits to extract the virial coefficients b_n, b_p, b_{nn}, b_{pp} and b_{np} of the gRMF model. The first-order coefficients receive a relativistic correction with

$$b_n = g_n k_2\left(\frac{m_n}{T}\right) , \tag{81}$$

$$b_p = g_p k_2\left(\frac{m_p}{T}\right) . \tag{82}$$

They depend on the temperature now. In the non-relativistic limit $T/m_i \to 0$ the correction will vanish due to the asymptotic expansion of the function k_2, cf. Eq. (65). Below we will show that these corrections are important and should be taken into account for an improved description of low-density nuclear matter. Similarly, there is a relativistic modification to the statistical corrections in b_{nn} and b_{pp}, i.e. Eqs. (19) and (20), respectively, and to the deuteron contribution to (22). From the comparison of (18) and (80), three independent relations for the channels nn, pp and np remain

$$-\frac{T}{\lambda_n^3}\left[b_{nn}+\frac{g_n}{2^{5/2}}k_2\left(2\frac{m_n}{T}\right)\right] = -\frac{T}{\lambda_{nn}^3}k_2\left(\frac{2m_n}{T}\right)\sum_l g_l^{(nn)} I_l^{(nn)} \tag{83}$$

$$= \frac{1}{2}\frac{g_n^2}{\lambda_n^6}\left[\left(C_\omega + C_\rho\right)k_2^2\left(\frac{m_n}{T}\right) - \left(C_\sigma + C_\delta\right)k_1^2\left(\frac{m_n}{T}\right)\right] ,$$

$$-\frac{T}{\lambda_p^3}\left[b_{pp}+\frac{g_p}{2^{5/2}}k_2\left(2\frac{m_p}{T}\right)\right] = -\frac{T}{\lambda_{pp}^3}k_2\left(\frac{2m_p}{T}\right)\sum_l g_l^{(pp)} I_l^{(pp)} \tag{84}$$

$$= \frac{1}{2}\frac{g_p^2}{\lambda_p^6}\left[\left(C_\omega + C_\rho\right)k_2^2\left(\frac{m_p}{T}\right) - \left(C_\sigma + C_\delta\right)k_1^2\left(\frac{m_p}{T}\right)\right] ,$$

$$-T\left[2\frac{b_{np}}{\lambda_n^{3/2}\lambda_p^{3/2}} - \frac{g_d}{\lambda_d^3}k_2\left(\frac{m_d}{T}\right)\exp\left(\frac{B_d}{T}\right)\right] \tag{85}$$

$$= -\frac{T}{\lambda_{np}^3}k_2\left(\frac{m_n+m_p}{T}\right)\sum_l\left[g_l^{(np1)}I_l^{(np1)} + g_l^{(np0)}I_l^{(np0)}\right]$$

$$= \frac{g_n g_p}{\lambda_n^3\lambda_p^3}\left[\left(C_\omega - C_\rho\right)k_2\left(\frac{m_n}{T}\right)k_2\left(\frac{m_p}{T}\right)\right.$$

$$\left. - \left(C_\sigma - C_\delta\right)k_1\left(\frac{m_n}{T}\right)k_1\left(\frac{m_p}{T}\right)\right]$$

that connect the virial integrals with the strengths C_m of the zero-density meson-nucleon couplings $\Gamma_m(0)$ of the gRMF model. The expected correction

factors $k_2(m_i/T)$ due to the relativistic effects were added to the VEoS part (expressed through virial integrals I_l^{ij}) of relations (83) to (85).

3.5. Temperature independent limit of consistency conditions

The consistency relations (83) to (85) were derived from a comparison of two fugacity expansions that are valid at low densities and finite temperatures, i.e. in the virial limit. These conditions arise from the contributions in the fugacity expansion that are quadratic in the fugacities. We perform an expansion of Eqs. (83) to (85) in powers of small T/m_i and keep the lowest-order terms which are independent of T. This is equivalent of taking the limit $T \to 0$ in (83) to (85). In this limit there are no relativistic corrections, only s-wave contributions are relevant and the limit (32) of the integral with the scattering lengths can be used. In the gRMF model the nucleon-nucleon interaction is identical in the nn and pp systems. Thus, the first two equations, (83) and (84) cannot be considered independent but should be combined. Denoting the scattering lengths in the s-wave channels explicitly with $a_{^1S_0}^{(nn)}$, $a_{^1S_0}^{(pp)}$, $a_{^1S_0}^{(np)}$ and $a_{^3S_1}^{(np)}$ and considering the degeneracy factors $g_n = g_p = 2$, $g_{^1S_0}^{(nn)} = g_{^1S_0}^{(pp)} = g_{^1S_0}^{(np)} = 1$ and $g_{^3S_1}^{(np)} = 3$, the two consistency conditions

$$C_\omega - C_\sigma = \pi \left\{ \frac{1}{2} \left[\frac{a_{^1S_0}^{(nn)}}{m_n} + \frac{a_{^1S_0}^{(pp)}}{m_p} \right] + \frac{m_n + m_p}{m_n m_p} \frac{a_{^1S_0}^{(np)} + 3a_{^3S_1}^{(np)}}{4} \right\} \tag{86}$$

and

$$C_\rho - C_\delta = \pi \left\{ \frac{1}{2} \left[\frac{a_{^1S_0}^{(nn)}}{m_n} + \frac{a_{^1S_0}^{(pp)}}{m_p} \right] - \frac{m_n + m_p}{m_n m_p} \frac{a_{^1S_0}^{(np)} + 3a_{^3S_1}^{(np)}}{4} \right\} \tag{87}$$

for the isovector and isoscalar meson couplings are obtained. The left side of Eqs. (86) to (87) corresponds to the gRMF expansion while the right side represents the virial expansion in the effective-range approximation.

With the coupling constants at zero density $\Gamma_m(0)$ and the meson masses m_m the coupling coefficients C_m can be calculated for different RMF models. In Table 1 the results are shown for the gRMF model with parametrization DD2 without δ meson following Ref. [25] and for a new density dependent RMF parametrization DD-MEδ from [39] based on ab-initio calculations in nuclear matter including a Lorentz scalar isovector δ meson.
In the DD2 parametrization the differences of the coupling coefficients are

Table 1: Coupling coefficients (79) in the DD2 parametrization of the gRMF model [25] and the DD-MEδ parametrization of Ref. [39].

Model	DD2	DD-MEδ
meson m	C_m [fm^2]	C_m [fm^2]
ω	17.250448	14.539639
σ	22.639364	19.443381
ρ	2.483932	6.017331
δ	–	3.462716

$C_\omega - C_\sigma = -5.39$ fm^2 and $C_\rho - C_\delta = 2.48$ fm^2, respectively. In contrast, the calculation with the scattering lengths from Ref. [35] gives $C_\omega - C_\sigma = -14.15$ fm^2 and $C_\rho - C_\delta = -9.61$ fm^2. It is obvious that the coupling coefficients of the gRMF model do not obey the consistency relations to guarantee the agreement with the VEoS at low densities.

For the recently developed parametrization DD-MEδ [39], the differences of the coupling coefficients turn out to be $C_\omega - C_\sigma = -4.90$ fm^2 and $C_\rho - C_\delta = 2.55$ fm^2. These numbers are close to those of the DD2 parametrization. There are still differences to the values required by the consistency conditions (86) and (87) and a more drastic modification of the low-density couplings seems to be necessary.

In the DD2 parameter fit of the gRMF approach a particular form of the density dependence of the coupling functions $\Gamma_m(\varrho)$ was assumed. The choice was motivated by results from Dirac-Brueckner calculations of nuclear matter [26]. However, the values at zero density are found from a not well constrained extrapolation to small densities. Only near the saturation density of symmetric nuclear matter they are well determined from model fits to the properties of atomic nuclei. Thus, in general, one could modify the density dependence of $\Gamma_m(\varrho)$ for all mesons m at low densities in order to satisfy the constraints (86) and (87). Since $C_\rho - C_\delta$ has to be negative, it is clear that the standard ω, σ and ρ mesons are not sufficient and a δ meson is needed in this case.

Since Eqs. (86) and (87) give only two relations for four coupling coefficients C_m, obtained from the consistency with the virial expansion, two further constraints are required to fix all couplings unambiguously. Hence, in addition to the virial constraints, we tried to fit the vacuum couplings

coefficients $\Gamma_m(0)$ by describing low-energy nucleon-nucleon scattering, i.e. experimentally determined NN phase shifts [33], simultaneously satisfying equations (86) and (87). The corresponding Schrödinger equation in coordinate space was solved using σ, ω, ρ and δ mesons with a one-boson exchange potential [40] in order to fit the coupling constants of the nucleon-meson interaction and to describe the experimentally known phase shifts and effective range parameters given in [35], [41]. The gradient terms in the potential lead to unphysical singularities at $r \to 0$, thus to avoid these singularities a certain cutoff was introduced as in [42]. Coupling constants derived in this way would serve as an additional constraint at zero densities, improving the density dependence of the coupling functions $\Gamma_m(\varrho)$. However, even when the contribution of the pion was included, that does not appear in the mean-field approximation, it was impossible to find a reasonable parametrization. Quite drastic modifications of the low-density meson-nucleon couplings and meson masses were required. This failure is not very surprising because the number of meson fields in the RMF model is much smaller than that in realistic NN potentials resulting in a smaller number of degrees of freedom. In addition, the meson fields in the RMF model do not represent real physical mesons and their masses, that are used as adjustable parameters, e.g. in case of the σ meson, are not identical to the true meson masses. Hence, we do not follow this approach but extend the gRMF model further.

4. Extension of the gRMF approach

The failure of the gRMF model to describe the virial limit suggests that a further extension of the approach is inevitable. In addition to the bound state two-body correlation, the deuteron, we introduce additional degrees of freedom in the grand canonical potential that represent the possible two-nucleon states, nn, pp and np, in the continuum. In the following, we will consider the isospin 0 and 1 channels for the np states separately. Each of the two-body channels is represented by a temperature dependent resonance energy ($\tilde{E}_{nn}$, $\tilde{E}_{pp}$, $\tilde{E}_{np0}$, $\tilde{E}_{np1}$) and a corresponding effective degeneracy factor ($\tilde{g}_{nn}$, $\tilde{g}_{pp}$, $\tilde{g}_{np0}$, $\tilde{g}_{np1}$). In general, the resonance energies and degeneracy factors do not necessarily have to be the same as the resonance energies of Eq. (24) or the standard degeneracy factors in Eqs. (19) to (22). Two-body correlations in the continuum are considered as two-body clusters with mass

$$\tilde{m}_{ij} = N_{ij} m_n + Z_{ij} m_p + \tilde{E}_{ij} \tag{88}$$

with a temperature dependent resonance energy $\tilde{E}_{ij}$. We assume that the energy shift of a cluster ΔB_{ij} that appears in the scalar self-energy (44) is identical to the binding energy shift of the deuteron ΔB_d for all continuum channels. Of course, this most simple choice can be substituted by improved descriptions in the future. The specific functional form of the medium-dependent energy shift will affect the form of the transition from very low densities, where the VEoS is applicable, to the high-density regime. However, for the low-density matching of the VEoS and gRMF model it is irrelevant.

The total rest mass of the cluster in the medium is given by

$$\tilde{M}_{ij} = \tilde{m}_{ij} + \Delta B_{ij} \; . \tag{89}$$

In case of the virial approach, the appearing masses are given by $m_{ij} = N_{ij} m_n + Z_{ij} m_p + E_{ij}$ and $M_{ij} = m_{ij}$, respectively. We include the effect of the resonance energies in the relativistic correction through the k_2 function and the definition of the thermal wave lengths $\lambda_{ij} = [2\pi/(M_{ij}T)]^{1/2}$ and similarly for $\tilde{\lambda}_{ij}$. With these modifications we can rederive consistency relations between this extended gRMF model and the VEoS.

The virial integrals (23) in the virial coefficients are represented by an exponential of the effective resonance energy as defined in (24). The two np channels are separated by requiring for the np isospin 1 channel a similar form as for the nn and pp channels. Comparing the fugacity expansion of the gRMF model with 2-body correlations with the VEoS at low densities, we finally obtain an extension of the relations (83) to (85) , where an additional term with temperature dependent resonance energy $\tilde{E}_{ij}(T)$ appears in the right-hand side of the Eqs. (90) to (91), i.e.

$$\begin{aligned} & -\frac{T}{\lambda_{ij}^3} k_2\left(\frac{M_{ij}}{T}\right) \hat{g}_{ij} \exp\left(-\frac{E_{ij}}{T}\right) \\ = \; & -\frac{T}{\tilde{\lambda}_{ij}^3} k_2\left(\frac{\tilde{M}_{ij}}{T}\right) g_{ij}^{(\mathrm{eff})} \exp\left(-\frac{\tilde{E}_{ij}}{T}\right) \\ & + \frac{1}{2}\frac{g_i g_j}{\lambda_i^3 \lambda_j^3}\Big[(C_\omega + C_\rho)\, k_2\left(\frac{m_i}{T}\right) k_2\left(\frac{m_j}{T}\right) \\ & - (C_\sigma + C_\delta)\, k_1\left(\frac{m_i}{T}\right) k_1\left(\frac{m_j}{T}\right)\Big] \end{aligned} \tag{90}$$

for the channels $ij = nn$, pp, $np1$ and

$$
\begin{aligned}
&-\frac{T}{\lambda_{np0}^3} k_2\left(\frac{M_{np0}}{T}\right) \hat{g}_{np0} \exp\left(-\frac{E_{np0}}{T}\right) \qquad (91)\\
&= -\frac{T}{\tilde{\lambda}_{np0}^3} k_2\left(\frac{\tilde{M}_{np0}}{T}\right) g_{np0}^{(\mathrm{eff})} \exp\left(-\frac{\tilde{E}_{np0}}{T}\right)\\
&\quad + \frac{1}{2}\frac{g_n g_p}{\lambda_n^3 \lambda_p^3}\Big[\left(C_\omega - 3C_\rho\right) k_2\left(\frac{m_n}{T}\right) k_2\left(\frac{m_p}{T}\right)\\
&\quad - \left(C_\sigma - 3C_\delta\right) k_1\left(\frac{m_n}{T}\right) k_1\left(\frac{m_p}{T}\right)\Big]
\end{aligned}
$$

for the channel $np0$. These consistency relations leave sufficient freedom to reproduce the exact VEoS at low densities in the gRMF model. There are different possibilities to achieve this goal depending on the choice of the zero-density couplings and on the choice of the effective resonance energies and degeneracy factors that represent the continuum contributions in the extended gRMF model. The structure on the left-hand side shares some similarities with the generalized Beth-Uhlenbeck approach in Section 2.4. One part of the effects of the two-body correlations is included in the explicit continuum contributions and the remaining part is covered by the mean-field terms. There is the freedom to shift the correlation strength between these terms rather arbitrarily. In the following, a few choices will be discussed.

In Section 3.5 the case without introducing explicit continuum channels in the gRMF model, i.e. shifting the full correlation strength into a redefinition of the vacuum couplings, turned out to be impossible. The other extreme is to represent the correlations by the introduction of the effective continuum states described by temperature dependent resonance energies $\tilde{E}_{ij}$ with medium corrections ΔB_{ij} as described above. In this case the contribution of the virial integral in the left-hand side of the Eqs. (90) and (91) is fully represented by the the resonance energies $\tilde{E}_{ij}$ in the first term in the right-hand side of these equations. Therefore the mean-field part has to vanish in the non-relativistic limit, leading to $C_\omega - C_\sigma = 0$ and $C_\rho - C_\delta = 0$. The coupling coefficients C_m in relations (86) to (87) were expressed through the virial integral taken in the effective range approximation. In the new relations, given above, the virial integral and thus the scattering lengths are implemented in the definition of the resonance energies $\tilde{E}_{ij}(T)$. Therefore, neglecting the term proportional to $g_{ij}^{(\mathrm{eff})} \exp\left(-\tilde{E}_{ij}/T\right)$ in the relations (90) and (91), we

recover equations (83) to (85), leading to the consistency conditions (86) to (87).

In order to fix the four couplings C_m unambiguously, we again tried to describe low-energy nucleon-nucleon scattering, by solving the Schrödinger equation with one-boson exchange potentials as described in Section 3.5 simultaneously with the two conditions on the couplings $C_\omega - C_\sigma = 0$, $C_\rho - C_\delta = 0$. We observed that the required coupling constants at zero density are drastically different in comparison with the previous values of the parametrization DD2 or DD-MEδ leading to problems such as a rather unphysical behavior of the EoS at low densities by similar reasons as in the first attempt at the end of Section 3.5. Consequently, this approach was discarded. It was not possible to describe both the NN scattering data and the VEoS simultaneously in this second choice for representing the continuum correlations.

Therefore the most straightforward way to fulfill the consistency relations (90) and (91) is to leave the density dependence of meson-nucleon couplings untouched as given by the gRMF model parametrization and to turn down the idea of an additional fit to NN scattering data, thus concentrating only on the reproduction of the VEoS. The effects of the two-body correlations are incorporated in the effective resonance energies that are chosen as identical to those of the VEoS, i.e. $\tilde{E}_{ij} = E_{ij}$. Then, the consistency relations (90) and (91) are seen as the defining equations for the effective degeneracy factors $g_{ij}^{(\mathrm{eff})}$ that now depend on temperature. In the non-relativistic limit, these equations simplify as

$$g_{nn}^{(\mathrm{eff})}(T) = \hat{g}_{nn} + \frac{g_n^2}{2T}\frac{\lambda_{nn}^3}{\lambda_n^6} C_1 \exp\left[\frac{E_{nn}(T)}{T}\right], \tag{92}$$

$$g_{pp}^{(\mathrm{eff})}(T) = \hat{g}_{pp} + \frac{g_p^2}{2T}\frac{\lambda_{pp}^3}{\lambda_p^6} C_1 \exp\left[\frac{E_{pp}(T)}{T}\right], \tag{93}$$

$$g_{np1}^{(\mathrm{eff})}(T) = \hat{g}_{np1} + \frac{g_n g_p}{2T}\frac{\lambda_{np1}^3}{\lambda_n^3\lambda_p^3} C_1 \exp\left[\frac{E_{np1}(T)}{T}\right], \tag{94}$$

$$g_{np0}^{(\mathrm{eff})}(T) = \hat{g}_{np0} + \frac{g_n g_p}{2T}\frac{\lambda_{np0}^3}{\lambda_n^3\lambda_p^3} C_0 \exp\left[\frac{E_{np0}(T)}{T}\right] \tag{95}$$

where

$$C_1 = C_\omega - C_\sigma + C_\rho - C_\delta\,, \tag{96}$$

$$C_0 = C_\omega - C_\sigma - 3\,(C_\rho - C_\delta) \tag{97}$$

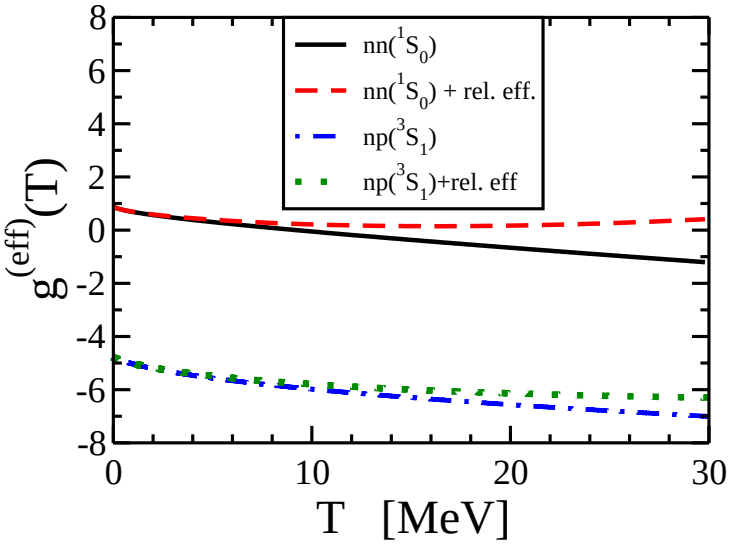

Figure 3: Temperature dependence of the effective degeneracy factors $g_{nn}^{(\mathrm{eff})}$ and $g_{np0}^{(\mathrm{eff})}$ with and without relativistic corrections.

are the relevant couplings in the two isospin channels. If $C_1 = C_0 = 0$ as was discussed before as a possible condition, we recover the standard degeneracy factors $\hat{g}_{ij}$ in the s-wave. The degeneracy factors on the right-hand side are $\hat{g}_{nn} = \hat{g}_{pp} = \hat{g}_{np1} = 1$ and $\hat{g}_{np0} = -3$, respectively. The negative sign for $\hat{g}_{np0}$ is related to the positive s-wave scattering length in this channel. Note that in the NSE description, cf. Subsection 2.3, the temperature dependence of the degeneracy factors follows from the inclusion of excited states of the nuclei. In our approach, it represents the contribution of the continuum states and thus is very similar.

In Fig. 3 the temperature dependence of the effective degeneracy factors is depicted for the scattering correlations in the nn and $np0$ channels. Because the curves for the pp and $np1$ channels are practically identical to the nn scattering case, they are not shown. The fully relativistic results as they follow from Eqs. (90) and (91) are compared with their non-relativistic limits (92) and (95), respectively. We see that the relativistic corrections caused by the k_1 and k_2 functions are minor at low temperatures but grow with the increase of temperature as expected, being larger for the case of nn scattering. The large relativistic correction in the effective degeneracy factors is caused by an accidental change of sign in the factor containing the coupling

coefficients in Eq. (90).

In the zero-temperature limit, the effective degeneracy factors are given by

$$g_{ij}^{(\mathrm{eff})}(0) = \hat{g}_{ij} - \frac{\hat{g}_{ij}}{g_{ij}} \frac{C_1}{2\pi a_{ij}} \frac{2m_i m_j}{m_i + m_j} , \tag{98}$$

$$g_{np0}^{(\mathrm{eff})}(0) = \hat{g}_{np0} - \frac{\hat{g}_{np0}}{g_{np0}} \frac{C_0}{2\pi a_{np0}} \frac{2m_n m_p}{m_n + m_p} \tag{99}$$

for the channels $ij = nn, pp, np1$ and $np0$, respectively, when the approximation (32) with the scattering length is used. Thus, there is still a difference as compared to $\hat{g}_{ij} = 1$ and $\hat{g}_{np0} = -3$, respectively, when the correction due to the meson couplings is not taken into account. This is a clear indication that the mean field effectively takes over a part of the correlations.

5. Neutron matter

In nuclear matter with arbitrary neutron to proton ratio, the two-body correlations in all nucleon-nucleon channels contribute to the thermodynamic properties and, in particular, the deuteron bound state dominates at low temperatures. The case is different for pure neutron matter where only the nn channel without a bound state is relevant. Thus, neutron matter is ideally suited to demonstrate the effects of the continuum correlations in the extension of the gRMF model. Before the general case of finite temperatures is discussed, we first consider in brief the case $T = 0$ in the limit of small densities.

5.1. Zero temperature limit

At zero temperature the Fermi momentum k_{F_n} defined through the neutron density $n_n = k_{F_n}^3/(3\pi^2)$ sets the scale for all results. Instead of an expansion in powers of the neutron fugacity at finite temperature, a series expansion in powers of k_{F_n} is the relevant method to study the low-density behavior of the EoS. In Ref. [43] it was shown that the energy per neutron E/N (without rest mass) at very small k_{F_n} can be expanded in a power series

$$\frac{E}{N} = E_{\mathrm{free}} \xi \tag{100}$$

with the power series

$$\xi = 1 + \frac{10}{9\pi}\zeta + \frac{4}{21\pi^2}(11 - 2\ln 2)\,\zeta^2 + \ldots \tag{101}$$

in the dimensionless parameter $\zeta = a_{^1S_0}^{(nn)} k_{F_n}$. Here $E_{\rm free} = 3k_{F_n}^2/(10m_n)$ is the energy per neutron of a non-interacting Fermi gas that defines the relevant energy scale. Because of the unnaturally large negative nn scattering length $a_{^1S_0}^{(nn)} \approx -18.8$ fm [35], the radius of convergence is unfortunately very small, i.e. $n_n \ll 243\pi/|10a_{^1S_0}^{(nn)}|^3 \approx 1.1 \cdot 10^{-4}$ fm^{-3}.

In the DD-RMF approach without effective contributions of two-body correlations, an expansion of the energy per neutron in powers of the Fermi momentum (see Appendix B) leads to

$$\frac{E}{N} = E_{\rm free}\xi_{\rm RMF} \tag{102}$$

with

$$\xi_{\rm RMF} = 1 + \frac{5}{9\pi^2}\left(C_\omega - C_\sigma + C_\rho - C_\delta\right) m_n k_{F_n} + \dots \,. \tag{103}$$

A comparison with Eq. (101) gives the relation

$$C_\omega - C_\sigma + C_\rho - C_\delta = \frac{2\pi}{m_n} a_{^1S_0}^{(nn)}. \tag{104}$$

This condition coincides with condition (83) for neutron matter, although it is derived in the low k_{F_n}/m_n limit for $T = 0$ whereas condition (83) in the $T \to 0$ limit of the finite-temperature virial expansion with vanishing convergence radius in density. From a physical point of view, this coincidence is not surprising since both approaches only use two-body scattering information. However, it is gratifying to find the coincidence from the two very different approaches. We find the values of -2.91 fm^2 and -2.35 fm^2 for $C_\omega - C_\sigma + C_\rho - C_\delta$ in the DD2 and DD-MEδ parametrizations, respectively. However, these are much smaller in modulus as compared to the required value of $2\pi a_{^1S_0}^{(nn)}/m_n = -24.83$ fm^2.

A particular situation arises in the unitary limit [44], i.e. if $a_{^1S_0}^{(nn)}$ approaches $-\infty$. Then the series expansion (101) can no longer be applied since the radius of convergence shrinks to zero. In fact, the energy per nucleon should scale as the energy per neutron of a non-interacting Fermi gas $E_{\rm free}$ with a universal constant ξ independent of k_{F_n}. The parameter $\xi_{\rm RMF}$ is independent of k_{F_n} in first-order only if the combination $C_\omega - C_\sigma + C_\rho - C_\delta$ diverges as $k_{F_n}^{-1}$. Hence a particular density dependence of at least one meson-nucleon coupling is required in this case.

In the nonlinear RMF model of Ref. [12] with nonlinear self-interactions of the scalar meson, a density dependence of the σ meson coupling was introduced for densities lower than a particularly chosen transition density with the aim to reproduce the energy per neutron for unitary neutron matter assuming $\xi = 0.44$ [45]. This condition required a divergence of $\Gamma_\sigma(n) \propto n^{-1/6}$ that is consistent with the expectation from Eq. (103). However, mixing the nonlinear RMF approach and the RMF model with density dependent and divergent couplings does not seem to be very natural. In our approach, we do not aim to describe the neutron matter EoS at zero temperature and low densities as a unitary Fermi gas (FG) but require consistency with the VEoS for $T > 0$.

5.2. Finite temperatures

We choose $T = 4$ MeV and $T = 10$ MeV as representative examples which illustrate the main effects due to interactions and correlations. Different approximations in the description will be compared, ranging from the ideal Fermi gas via the virial approach to the gRMF model. Nucleons are treated as Fermions and clusters as Maxwell-Boltzmann particles because they appear at high temperatures with low abundancies when deviations from the correct Bose-Einstein statistics are negligible.

There are two quantities that exhibit finite low-density limits and hence are very advantageous for a comparison of the models: the ratio of the pressure over total particle number density p/n and of the internal energy per baryon $E/N = \varepsilon/n - m_n$ (without the rest mass of the neutron) with the energy density

$$\varepsilon = \frac{1}{V}\left(\Omega + TS\right) + \sum_{i=n,nn} \tilde{\mu}_i n_i \tag{105}$$

that can be calculated from the grand canonical potential Ω, the entropy S and the relativistic chemical potentials $\tilde{\mu}_i$. The sum contains the contribution of the neutrons and that of the correlated two-neutron continuum. Correspondingly, the total particle number density n is the sum

$$n = n_n + 2n_{nn} \tag{106}$$

and the mass fraction of correlated two-neutron states is defined by

$$X_{nn} = \frac{2n_{nn}}{n_n + 2n_{nn}}\,. \tag{107}$$

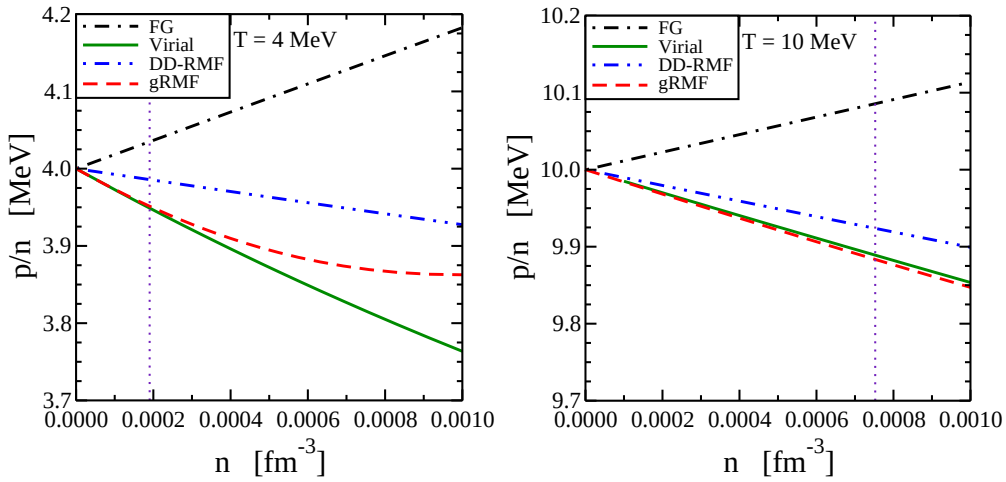

Figure 4: Ratio of pressure over total particle number density, p/n, of neutron matter as a function of the total density n for temperatures of $T = 4$ MeV (left) and $T = 10$ MeV (right). Vertical dotted lines indicate the density where $n\lambda_n^3 = 1/10$.

For an ideal gas with Maxwell-Boltzmann statistics and non-relativistic kinematics, we have the simple result that $p/n = T$ and $E/N = 3T/2$ are independent of the density of the system and trivially $X_{nn} = 0$. Deviations from these values indicate the effects of correlations and interactions.

5.2.1. Low densities

In Figures 4 and 5 the two quantities p/n and E/N, respectively, are depicted for the two selected temperatures as a function of the total particle number density n in different theoretical approaches. In case of the relativistic Fermi gas (see FG-curve), effects of the Pauli principle are taken into account leading to an increase of the pressure and of the energy per neutron as compared to the ideal Boltzmann gas. The limit $\lim_{n\to 0}(p/n) = T$ is not affected by statistical corrections or relativistic kinematics since the k_2 factors cancel in the lowest order of the fugacity expansion. This is easily seen considering the ratio $p = -\Omega/(Vn)$ using Eqs. (62) and (64). In contrast, the relativistic correction factor k_2 in Eq. (64) modifies the relation between the neutron density and neutron chemical potential appearing in Eq. (105) and thus $\lim_{n\to 0}(E/N) > 3T/2$ in figure 5. The relativistic corrections become larger with increasing temperature. The shift of E/N at zero density can be estimated as $2T^2/m_n$.

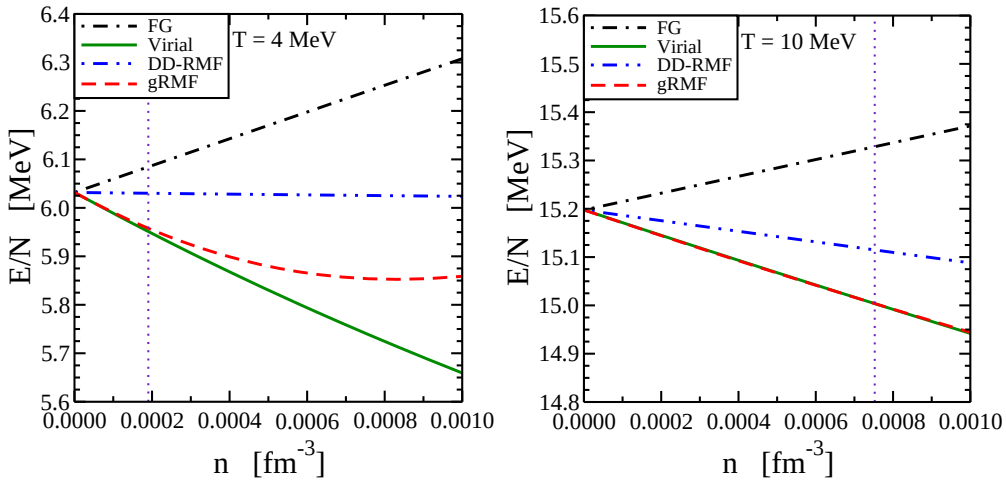

Figure 5: Internal energy per baryon (without contribution of the neutron rest mass) in neutron matter as a function of the total particle number density n for temperatures of $T = 4$ MeV (left) and $T = 10$ MeV (right). Vertical dotted lines indicate the density where $n\lambda_n^3 = 1/10$.

The VEoS predicts a dependence of p/n and E/N on the density with a negative slope. This is the effect of the correlations induced by the nn interaction. The vertical lines in Figures 4 and 5 denote the density n where $n\lambda_n^3 = 1/10$. At densities above this value, higher-order contributions to the VEoS, that are not considered in the fugacity expansion up to second order, can be expected to contribute significantly. Figure 5 also demonstrates that the virial corrections at low densities are smaller than the relativistic correction that leads to an overall shift.

The curves of the DD-RMF model with DD2 parametrization without correlations lie between the VEoS and the FG results. They do not show the correct dependence given by the VEoS at low densities. When the nn correlations are taken into account in the gRMF model with the quadratic form of the energy shift (see next subsection) the low-density behavior of the VEoS is nicely reproduced. Only at higher densities, medium effects, that are not incorporated in the VEoS, lead to a deviation. The precise density dependence of the deviation will depend on the choice of the functional form of the energy shift, but the agreement in the low-density limit is not affected. Obviously, deviations of the gRMF EoS from the VEoS start to become more important with increasing density at lower temperatures.

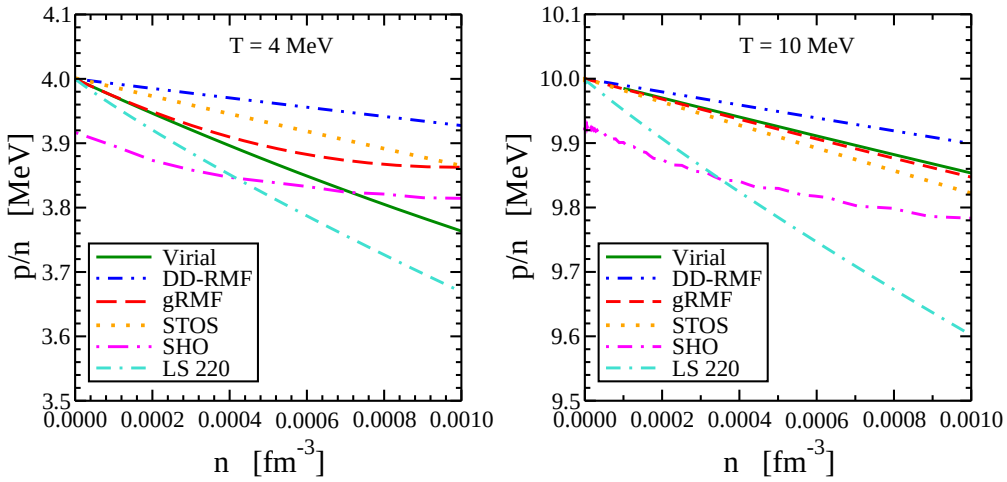

Figure 6: Ratio of pressure over total particle number density, p/n, of neutron matter as a function of the density n for temperatures of $T = 4$ MeV (left) and $T = 10$ MeV (right) in different models. See text for details.

It is also worthwhile to compare the predictions of the VEOS, the original DD-RMF and gRMF models in the DD2 parametrization with the results of other approaches used in astrophysical applications. We examine two other RMF models that employ nonlinear self-interactions of the mesons: the model of Shen, Horowitz and O'Connor (SHO) [15] with the FSUG-old parametrization and the model of Shen, Toki, Oyamatsu and Sumiyoshi (STOS) [16] with the parameter set TM1. In addition, the non-relativistic Lattimer-Swesty EoS with incompressibility $K = 220$ MeV (LS 220) is considered.

In Figure 6 the density dependence of the quantity p/n at $T = 4$ MeV and $T = 10$ MeV is depicted for all models below 0.001 fm^{-3}. The curves of the STOS model, that does not include two-body nn correlations, are surprisingly close to the exact VEoS line for $T = 10$ MeV, but do not reproduce it exactly. The deviations are larger at $T = 4$ MeV and the close agreement seems to be accidental for $T = 10$ MeV. The SHO approach with the FSUG-old parametrization claims to be constructed such that the case of unitary neutron matter is reproduced at low densities by introducing a particular density dependent coupling of the σ meson, see the discussion at the end of Subsection 5.1. A large deviation from the VEoS result can be seen in Fig. 6 and the correct low-density limit for p/n is not reproduced. Furthermore,

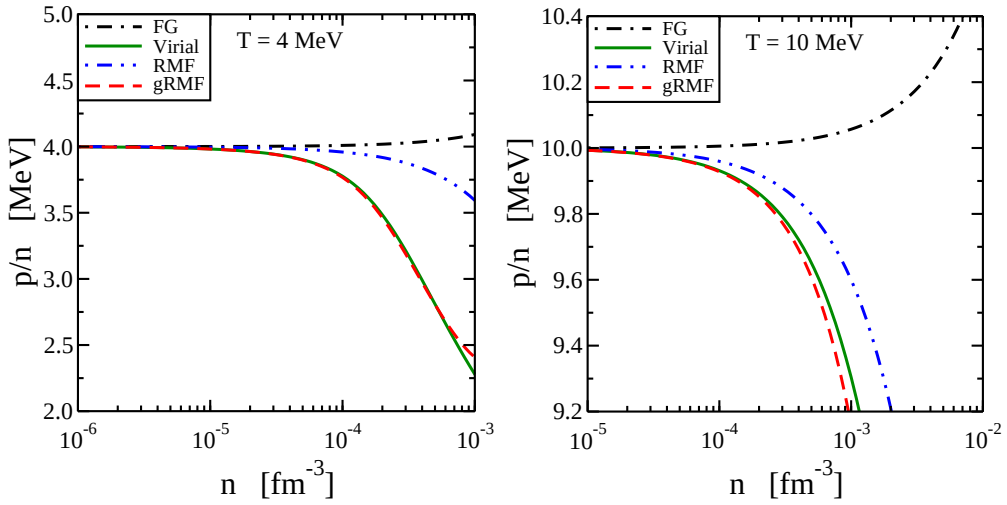

Figure 7: Ratio of pressure over total particle number density, p/n, of symmetric nuclear matter as a function of the total density n for temperatures of $T = 4$ MeV (left) and $T = 10$ MeV (right).

the tabulated data exhibit some oscillations that are probably related to the choice of the interpolation procedure [46]. The LS EoS shows a much larger negative slope of p/n as a function of n as compared to the other models but reproduces the correct ideal gas limit.

6. Symmetric nuclear matter

In contrast to neutron matter, where only neutron scattering correlations contribute to the thermodynamical quantities, all correlations of neutrons and protons in scattering and bound states should be taken into account in symmetric matter. At low densities, two-body correlations will be most important, but with increasing density also many-body correlations, in particular the appearance of clusters, i.e. many-body bound states, are relevant. Presently we include contributions from $nn(^1S_0)$, $np(^1S_0)$, $pp(^1S_0)$ and $np(^3S_1)$ scattering channels and clusters with $A \leq 4$ in our calculations. In the gRMF model light clusters (deuteron, triton, helion and α-particle) are introduced as additional degrees of freedom with temperature and density dependent binding energy shifts given in Ref. [25]. Because we do not consider the formation of nuclei with mass numbers $A > 4$ the present model can

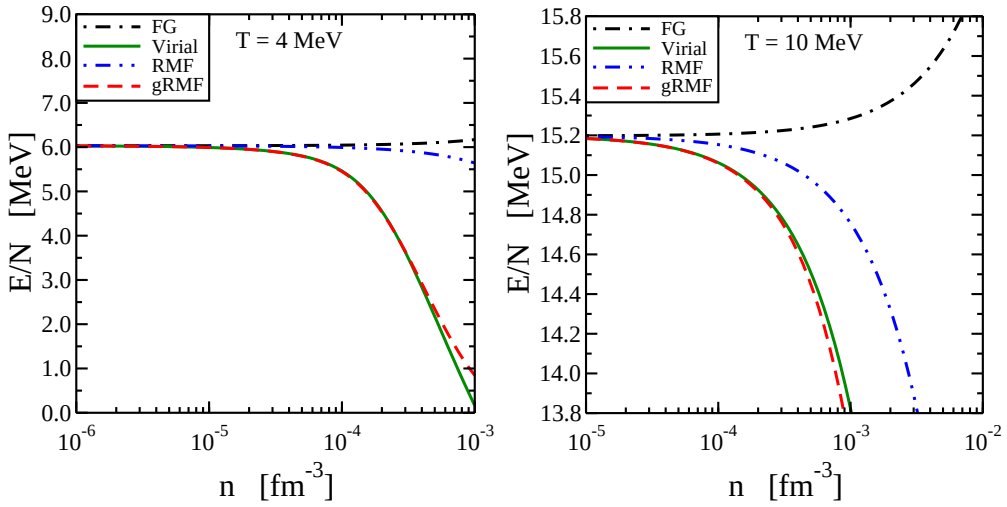

Figure 8: Internal energy per baryon (without contribution of the neutron rest mass) in symmetric nuclear matter as a function of the total particle number density n for temperatures of $T = 4$ MeV (left) and $T = 10$ MeV (right).

only be applied to rather low densities where the fraction of heavier clusters can be neglected.

6.1. Low densities

Similar as in the case of neutron matter, Figures 7 and 8 depict the quantities p/n and E/N, calculated in different approaches, for $T = 4$ MeV and $T = 10$ MeV as a function of the total particle number density n. The extended gRMF model very well reproduces the VEoS at low densities, deviating from it with increasing density and lower temperature due to medium effects. Note that in the depicted results of the VEoS calculation the same nuclei are considered as in the gRMF model. It is also worth noticing that the standard RMF calculation without clusters and the extended gRMF model differ substantially. Again, we see the effect of the relativistic corrections on the internal energy per baryon E/N in comparison with the ideal gas limit. In contrast to the neutron matter case, where scattering correlations are essential for reproducing the VEoS, in symmetric matter the main contribution is caused by the appearance of bound states with positive binding energy.

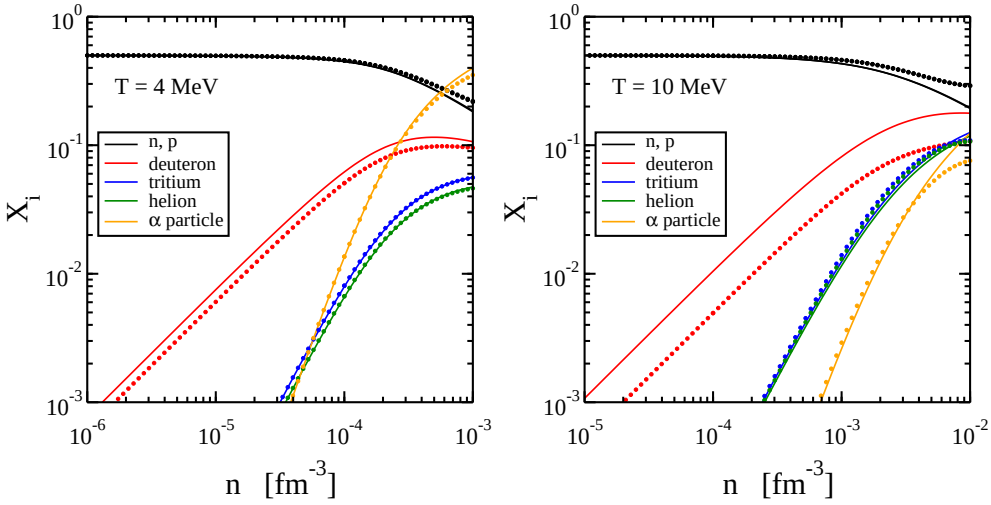

Figure 9: Particle fractions X_i of nucleons and light clusters in symmetric nuclear matter as a function of the density n for temperatures of $T = 4$ MeV (left) and $T = 10$ MeV (right). Solid lines correspond to the VEoS and dotted lines to the gRMF model.

6.2. Composition

It is worthwhile to study the detailed composition of symmetric nuclear matter, comparing the fractions of various particles. In Figure 9 particle fractions $X_i = A_i n_i/n$ of nucleons and light clusters are shown for $T = 4$ MeV and $T = 10$ MeV for gRMF (dotted lines) and VEoS (solid lines) models. The deuteron fraction X_d contains the contribution of the bound state and the isospin singlet np scattering channel. As is seen from the figures, in symmetric matter higher mass clusters become more important with increasing densities. One notes that the particle fraction for deuterons in the VEoS and gRMF models are substantially different, especially in case for $T = 10$ MeV. This behavior is caused by the fact that in the gRMF model part of the two-body correlation strength is shifted to the mean field, thus reducing the contribution of the original two-body correlations. The same effect will be observed in case of neutron matter for the particular case of nn correlations, see Section 7. We also notice different slopes of the curves for light clusters, with the α particle having the steepest inclination. The reason is that at low total densities cluster densities are proportional to fugacities in a certain power, e.g. $n_d \sim z^2$, $n_t \sim z^3$ and $n_\alpha \sim z^4$ with $z = z_n \approx z_p$ in symmetric nuclear matter. The overall scaling of the cluster fractions at low

densities is determined by the cluster binding energies. At densities n above 10^{-4} fm^{-3} and 10^{-3} fm^{-3} for $T = 4$ MeV and $T = 10$ MeV, respectively, heavier nuclei will contribute significantly to the composition in symmetric nuclear matter and they have to be incorporated in the model calculations. Hence, it is not reasonable to discuss the transition to higher densities in the present description of symmetric nuclear matter. The case of pure neutron matter is presented in the next section.

7. Higher densities

In subsection 5.2.1 it was demonstrated that the gRMF approach with effective nn scattering correlations reproduces the low-density limit of the VEoS for thermodynamical quantities such as p/n and E/N. With increasing density, the VEoS approach is no longer applicable and a smooth transition of the gRMF predictions to the DD-RMF results with neutrons as quasi-particles is expected. The details of this transition are affected by several ingredients of the gRMF model that are not constrained by the low-density expansion: the strength of the cluster-meson couplings (45), the shift ΔB_{nn} of the effective resonance energy E_{nn} and possible contributions from three, four, ... and many-neutron correlations. In the following, only the variation of the transition with different choices of ΔB_{nn} will be discussed. The strength of the cluster-meson couplings is kept as given in the original gRMF model and described in Section 3.

When the total density of neutron matter increases, the contribution of the nn cluster in the gRMF model will be affected by the applied shift to the resonance energy that represents the continuum correlations. The functional dependence of the energy shift ΔB_i of a cluster i in (44) with temperature T and the meson fields ω and σ is not determined by the low-density considerations. Here, we explore three different choices. Similar as in Ref. [25], we write

$$\Delta B_i = f[n_i^{(\mathrm{eff})}]\delta B_i(T) \tag{108}$$

with a function f that depends on the effective density

$$n_i^{(\mathrm{eff})} = \frac{m_\omega^2}{\Gamma_\omega(0)}\omega + \frac{N_i - Z_i}{A_i}\frac{m_\rho^2}{\Gamma_\rho(0)}\rho \tag{109}$$

and a temperature dependent factor $\delta B_i(T)$. At low effective densities, ΔB_i should be linear in $n_i^{(\mathrm{eff})}$ and an obvious choice is $f = n_i^{(\mathrm{eff})}$. In Ref. [25] the

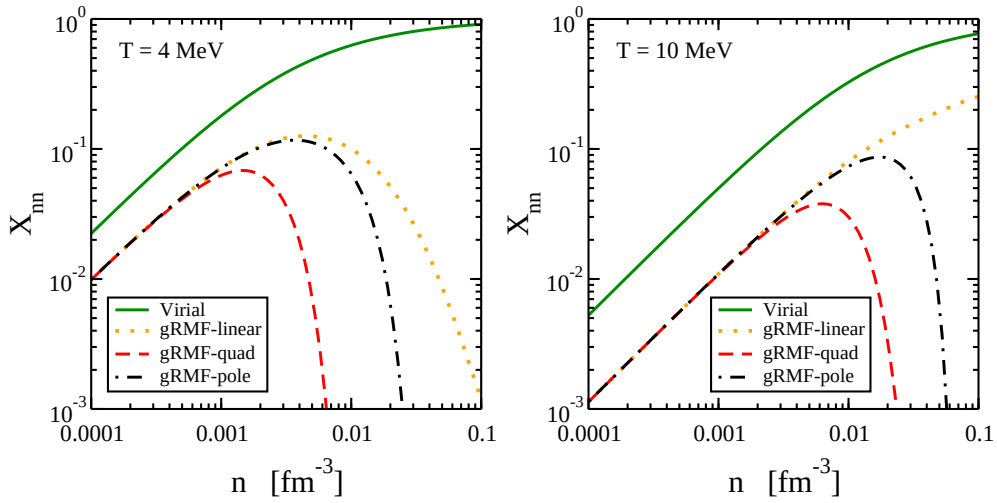

Figure 10: Mass fraction X_{nn} of the two-neutron correlation state in neutron matter as a function of the density n for temperatures of $T = 4$ MeV (left) and $T = 10$ MeV (right).

quadratic form

$$f = n_i^{(\mathrm{eff})} \left[1 + \frac{1}{2} \frac{n_i^{(\mathrm{eff})}}{n_i^{(0)}} \right] \tag{110}$$

was used for the light clusters in order to obtain a stronger suppression of the cluster abundancies with increasing density. The density scale $n_i^{(0)} = B_i^{(\mathrm{vac})}/\delta B_i(T)$ is set by the vacuum binding energy $B_i^{(\mathrm{vac})}$. Another possible choice is the pole form

$$f = \frac{n_i^{(\mathrm{eff})} n_{\mathrm{sat}}}{n_{\mathrm{sat}} - n_i^{(\mathrm{eff})}} \tag{111}$$

for $n_i^{(\mathrm{eff})}$ smaller than the saturation density n_{sat} of the gRMF model resulting in a complete dissolution of the cluster when n_{sat} is approached from below because $\lim_{n \to n_{\mathrm{sat}}} f = \infty$.

The evolution of the two-neutron mass fraction

$$X_{nn} = 2n_{nn}/(n_n + 2n_{nn}) \tag{112}$$

with increasing total density is depicted in Figure 10 for the VEoS and the gRMF model with the linear, quadratic and pole form of the energy shift ΔB_{nn}, respectively. We assume $\delta B_{nn}(T) = \delta B_d(T)$ and set the density scale

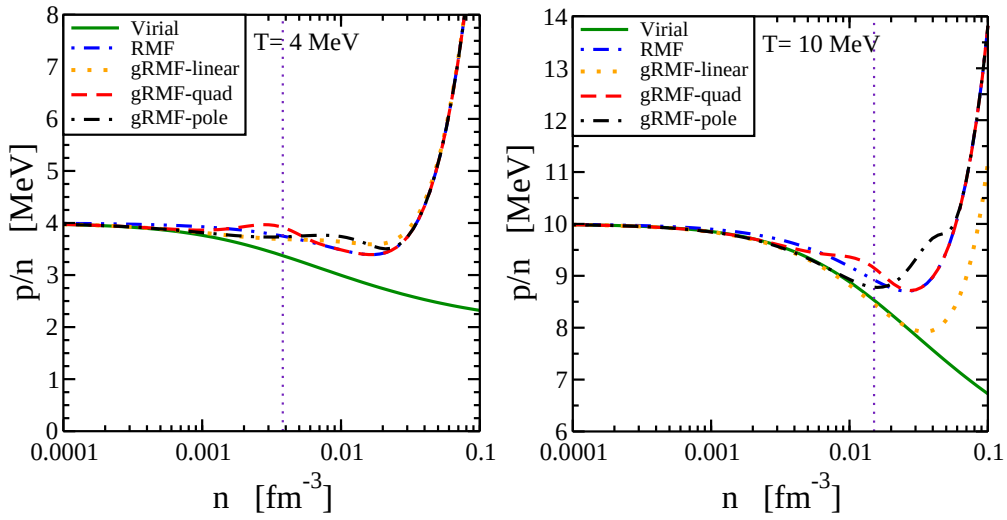

Figure 11: Ratio of pressure over total particle number density, p/n, of neutron matter as a function of the density n for temperatures of $T = 4$ MeV (left) and $T = 10$ MeV (right). Vertical dotted lines indicate the density where $n\lambda_n^3 = 1$.

$n_{nn}^{(0)} = n_d^{(0)} = B_d^{(\mathrm{vac})}/\delta B_d(T)$ with the deuteron values for the quadratic dependence. The nn fraction in the VEoS model rises monotonously with the total density reaching unrealistically high values much beyond the range of applicability of the approach. At low densities, the nn fractions for the different choices of the energy shift in the gRMF model agree perfectly with each other. They exhibit the same slope as the VEoS result. In general, the nn mass fraction at low densities is larger for the lower temperature but the two-neutron cluster dissolves earlier with increasing total density. The maximum mass fraction and range of cluster dissolution depends sensitively on the form of the energy shift ΔB_{nn}. There are substantial variations that need to be constrained in future investigations. On an absolute scale, the gRMF predictions for X_{nn} are substantially smaller than those of the VEoS at low densities. This difference is caused by the fact that in the gRMF approach the correlations of quasiparticles are considered and part of the correlation strength is contained in the self-energies, cf. the generalized Beth-Uhlenbeck approach in Subsection 2.4. The distribution of correlations between the explicit contribution from the cluster state and the implicit contribution via the self-energies depends on the nucleon-meson couplings at zero density of the particular gRMF parametrization.

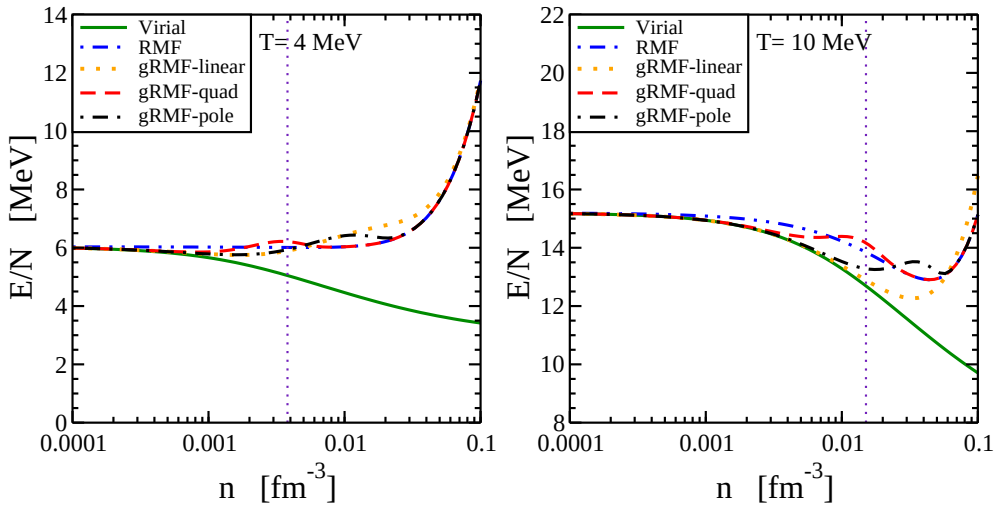

Figure 12: Internal energy per baryon (without contribution of the neutron rest mass) in neutron matter as a function of the total particle number density n for temperatures $T = 4$ MeV (left) and $T = 10$ MeV (right). Vertical dotted lines indicate the density where $n\lambda_n^3 = 1$.

The dependence of the quantities p/n and E/N in neutron matter on the total density is shown in Figures 11 and 12 for temperatures $T = 4$ MeV and $T = 10$ MeV and a wider range of densities compared to that shown in Figures 4 and 5. The vertical lines in Figures 11 and 12 denote the density n where $n\lambda_n^3 = 1$. In the low-density limit, all gRMF calculations reproduce the VEoS predictions by construction but deviate from the DD-RMF model that does not take cluster formation into account. At higher densities, the VEoS fails to predict the strong increase of the pressure and energy per neutron caused by the short-range repulsive nn interaction. The transition of the gRMF results at low densities to the DD-RMF curve at higher densities substantially depends on the choice of the energy shift ΔB_{nn} for the effective resonance energy E_{nn}. A distinctive bump in p/n and E/N appears that is correlated with the sudden dissolution of the two-body clusters as depicted in Figure 10. This feature was already observed in Ref. [25] for symmetric nuclear matter including only the bound states of light clusters. The origin of this structure is related to the contribution with the derivatives of the energy shifts in the ω and ρ-meson field equations (55) and (56). The functional form of the density dependence and absolute scale of the meson-cluster

coupling strengths Γ_{im} from (45) and (46) will also have an impact on the detailed form of the transition from the low-density limit to higher densities. In this work, only the most simple choice of the factor g_{im}, proportional to the number of nucleons in the cluster, was examined. Further investigations are needed to fix the cluster-meson couplings and the energy shifts less ambiguously. Correlations beyond two-neutron states, that are not considered for neutron matter in the present approach, could also modify the features in the quantities p/n and E/N.

8. Conclusions

In this paper, an extension of the generalized relativistic mean-field model with density dependent couplings was developed by requiring the consistency of the finite-temperature equation of state at low densities with the virial equation of state that is a model independent benchmark in this limit. For this purpose, new degrees of freedom were introduced in the generalized RMF approach that represent two-nucleon correlations in the continuum. These clusters can be considered as quasiparticles like bound nuclei. They are characterized by medium-dependent effective resonance energies with temperature dependent effective degeneracy factors.

From the comparison of the fugacity expansions of both the relativistic mean-field and virial equation of state models, consistency relations were derived that contain the nucleon-nucleon scattering phase shifts, the relativistic mean-field nucleon-meson coupling constants, the resonance energies and effective degeneracy factors of the clusters. Various limits were investigated for the choice of the relevant parameter functions and their dependence on the thermodynamical quantities. For a successful application of the approach, the density dependence of the original relativistic mean field model was kept and not modified at low densities. The effective resonance energies were taken as given by the calculation with the scattering phase shifts and the effective degeneracy factors were assumed to be temperature dependent similar as in the case of the nuclear statistical equilibrium model with thermally excited nuclei.

The example of neutron matter was studied in detail for different temperatures. Relativistic effects were found to become important with increasing temperature even at very low densities. The extended generalized relativistic mean-field model smoothly interpolates between the correct low- and high-density limits describing the dissolution of the clusters. However, the precise

form of the transition depends on the coupling strength of the clusters to the meson fields and the energy shift of the resonance energies. These quantities are not fixed by the low-density constraints and the consequences of different choices were investigated. This point deserves more studies in the future. In the case of symmetric nuclear matter the formation of many-body bound states is crucial for a realistic description of correlations.

The proposed extension of the generalized relativistic mean-field model is rather general and can also be applied to other mean-field approaches that aim at describing the equation of state of nuclear matter. In the present work, only two-particle correlations were considered. Bound states of light clusters with mass numbers $A \leq 4$ can be readily included as in Ref. [25]. A further extension to heavier nuclei with medium-dependent binding energies and finite-temperature excitations is also possible and corresponding work is in progress. For astrophysical applications, further contributions to the EoS than those considered in this work have to be included in the model. E.g. electrons, muons, photons, mesons etc. need to be considered which also change the behavior of various thermodynamical quantities in the low-density limit. Finally, equation of state tables with the thermodynamical properties and the composition of nuclear matter for a broad range in temperature, density and proton-neutron asymmetry can be generated for astrophysical simulations of, e.g., core-collapse supernovae.

Acknowledgments

The authors are grateful to D. Blaschke, T. Fischer, M. Hempel, T. Klähn, G. Röpke, A. Schwenk, K. Vantournhout and H.H. Wolter for discussions and comments during various stages of the work. We thank M. Oertel for providing the data of the Lattimer-Swesty EoS. The authors thank K. Langanke and B. Friman for continuous interest in this work. This research was supported by the DFG cluster of excellence 'Origin and Structure of the Universe' and by CompStar, a Research Networking Programme of the European Science Foundation (ESF). M.V. acknowledges support by the Helmholtz Graduate School for Hadron and Ion Research (HGS-HIRe). S.T. received support from the Helmholtz International Center for FAIR (HIC for FAIR) within the framework of the LOEWE program launched by the state of Hesse via the Technical University Darmstadt and from the Helmholtz Association (HGF) through the Nuclear Astrophysics Virtual Institute (VH-VI-417).

Appendix A. Virial equation in our model and in Ref. [18]

The authors of Ref. [18] use a slightly different definition of some quantities in their approach to the non-relativistic VEoS compared to the ones we use in Section 2. In order to facilitate the comparison, we indicate the correspondence of the two formulations. Quantities of Ref. [18] are indicated by a $\check{}$ in the following.

The single-particle partitions functions are defined in the same way, i.e. $Q_i = \check{Q}_i$ for nucleons and α-particles, however, there is a small difference in the thermal wavelengths because the neutron and proton mass are assumed to be equal $\check{m} = \check{m}_n = \check{m}_p$ in Ref. [18] and the α-particle mass is set to $\check{m}_\alpha = 4\check{m}$ without considering the binding energy as in Eq. (40). Similarly, for the non-relativistic chemical potentials the relation $\check{\mu}_\alpha = 2\check{\mu}_n + 2\check{\mu}_p$ is used instead of $\mu_\alpha = 2\mu_n + 2\mu_p - B_\alpha$ in our case. Nevertheless, the fugacities are identical. The main differences stem from the definition of the many-body partition functions. In Eq. (1) we place factors $1/n!$ in front of the n-body terms. Consequently $\check{Q}_{ij} = Q_{ij}/2$. Comparing Eq. (5) with Eq. (11) in [18], we identify

$$\check{b}_n = b_{nn}/2 = b_{pp}/2, \qquad \check{b}_{pn} = b_{pn}/2 \tag{A.1}$$

and

$$\check{b}_\alpha = b_{\alpha\alpha}, \qquad \check{b}_{\alpha n} = b_{\alpha n}/\sqrt{8} = b_{\alpha p}/\sqrt{8}\,. \tag{A.2}$$

In Eq. (16) we use the c.m. energy E as the integration variable. In contrast, in Ref. [18] the laboratory energies $\check{E} = 2E$ are used in Eqs. (19), (22) and (24) and the integrals are transformed with the help of a partial integration with respect to $\check{E}$. Noting that $\check{b}_{pn} = \check{b}_{\mathrm{nuc}} - \check{b}_n$ in Ref. [18], the formulas given there for $\check{b}_n$, $\check{b}_{pn}$ and $\check{b}_\alpha$ are consistent with the relations (A.1) and (A.2). For the virial coefficient $\check{b}_{\alpha n}$, the authors of Ref. [18] use the nucleon laboratory energy $\check{E} = 5E/4$ as integration variable. The expression (26) in Ref. [18], however, is a factor two too large to be consistent with the relation given in (A.2). This discrepancy was already noted in Ref. [28].

Appendix B. Zero temperature low-density limit in the gRMF model

In the case of pure neutron matter at zero temperature, all relevant thermodynamical quantities can be represented analytically as a function of the

Fermi momentum k_{F_n}. The energy density ε of pure neutron matter without contributions of the rest mass reads, cf., e.g., Ref. [26],

$$\begin{aligned}\varepsilon &= \frac{3}{4}\sqrt{k_{F_n}^2+(m_n-S_n)^2}\,n_n+\frac{1}{4}(m_n-S_n)\,n_n^{(s)} \\ &+\frac{1}{2}\left[\frac{\Gamma_\omega^2(n_n)}{m_\omega^2}+\frac{\Gamma_\rho^2(n_n)}{m_\rho^2}\right]n_n^2+\frac{1}{2}\left[\frac{\Gamma_\sigma^2(n_n)}{m_\sigma^2}+\frac{\Gamma_\delta^2(n_n)}{m_\delta^2}\right][n_n^{(s)}]^2\end{aligned} \tag{B.1}$$

where the scalar neutron density is given by

$$n_n^{(s)}=\frac{3}{2x^3}f(x)\,n_n \tag{B.2}$$

with the function

$$f(x)=x\sqrt{1+x^2}-\ln\left(x+\sqrt{1+x^2}\right) \tag{B.3}$$

that depends on the dimensionless parameter $x=k_{F_n}/(m_n-S_n)$. We define the derivative of the function (B.3), $f'=2x^2/\sqrt{1+x^2}$, and use the expansion

$$(1+z)^\alpha = \sum_{k=0}^{\infty}\frac{\Gamma(\alpha+1)}{k!\Gamma(\alpha+1-k)}z^{2k} \tag{B.4}$$

to rewrite equation (B.2) after integration as

$$\frac{n_n^{(s)}}{n_n} = 1-\frac{3}{10}\left[\frac{k_{F_n}}{m_n-S_n}\right]^2+\frac{9}{56}\left[\frac{k_{F_n}}{m_n-S_n}\right]^4+\ldots \tag{B.5}$$

Substituting $n_n^{(s)}$ in (B.1) by (B.5) and doing subsequent expansions in powers of k_{F_n} we arrive at expression (100) for the energy per neutron.

References

[1] T. Klähn et al., Phys. Rev. C 74 (2006) 035802.

[2] H.-Th. Janka, K. Langanke, A. Marek, G. Martínez-Pinedo, B. Mueller, Phys. Rep. 442 (2007) 38.

[3] N.K. Glendenning, *Compact stars: Nuclear physics, particle physics, and general relativity*, Springer, New York, 2000.

[4] J.M. Lattimer, M. Prakash, Science 304 (2004) 536.

[5] K. Sumiyoshi, G. Röpke, Phys. Rev. C 77 (2008) 055804.

[6] J.M. Lattimer, F.D. Swesty, Nucl. Phys. A 535 (1991) 331.

[7] H. Shen, H. Toki, K. Oyamatsu, K. Sumiyoshi, Prog. Theor. Phys. 100 (1998) 1013.

[8] H. Shen, H. Toki, K. Oyamatsu, K. Sumiyoshi, Nucl. Phys. A 637 (1998) 435.

[9] C. Ishizuka, A. Ohnishi, K. Tsubakihara, K. Sumiyoshi, J. Phys. G 35 (2008) 085201.

[10] A. Onishi, K. Tsubakihara, K. Sumiyoshi, C. Ishizuka, S. Yamada, H. Suzuki, Nucl. Phys. A 835 (2010) 374.

[11] M. Hempel, J. Schaffner-Bielich, Nucl. Phys. A 837 (2010) 210.

[12] G. Shen, C.J. Horowitz, S. Teige, Phys. Rev. C 82 (2010) 015806.

[13] G. Shen, C.J. Horowitz, S. Teige, Phys. Rev. C 82 (2010) 045802.

[14] G. Shen, C.J. Horowitz, S. Teige, Phys. Rev. C 83 (2011) 035802.

[15] G. Shen, C.J. Horowitz, E. O'Connor, Phys. Rev. C 83 (2011) 065808. `http://cecelia.physics.indiana.edu/gang_shen_eos/FSU/fsu.html`

[16] H. Shen, H. Toki, K. Oyamatsu, K. Sumiyoshi, ApJS 197 (2011) 20. `http://user.numazu-ct.ac.jp/~sumi/eos/`

[17] C.J. Horowitz, A. Schwenk, Phys. Lett. B 638 (2006) 153.

[18] C.J. Horowitz, A. Schwenk, Nucl. Phys. A 776 (2006) 55.

[19] E. O'Connor, D. Gazit, C.J. Horowitz, A. Schwenk, N. Barnea, Phys. Rev. C 77 (2007) 055803.

[20] Y.K. Gambhir, P. Ring, A. Thimet, Ann. Phys. (N.Y.) 198 (1990) 132.

[21] B.D. Serot, J.D. Walecka, Adv. Nucl. Phys. 16 (1996) 1.

[22] M. Bender, P.-H. Heenen, P.-G. Reinhard, Rev. Mod. Phys. 75 (2003) 121.

[23] E.E. Kolomeitsev, D.N. Voskresensky, Nucl. Phys. A 759 (2005) 373.

[24] J. Margueron, E. van Dalen, C. Fuchs, Phys. Rev. C 76 (2007) 034309.

[25] S. Typel, G. Röpke, T. Klähn, D. Blaschke, H.H. Wolter, Phys. Rev. C 81 (2010) 015803.

[26] S. Typel, H.H. Wolter, Nucl. Phys. A 656 (1999) 331.

[27] R. Dashen, S. Ma, H.J. Bernstein, Phys. Rev. 187 (1969) 345.

[28] S. Mallik, J.N. De, S.K. Samaddar, S. Sarkar, Phys. Rev. C 77 (2008) 032201.

[29] G.E. Beth, E. Uhlenbeck, Physica 3 (1936) 729.

[30] G.E. Beth, E. Uhlenbeck, Physica 4 (1937) 915.

[31] A. Pais, G.E. Uhlenbeck, Phys. Rev. 116 (1959) 250.

[32] G. Audi, A.H. Wapstra, C. Thibault, Nucl. Phys. A 729 (2003) 337.

[33] V.G.J. Stoks, R.A.M. Klomp, M.C.M. Rentmeester, J.J. de Swart, Phys. Rev. C 48 (1993) 792; see also http://nn-online.org.

[34] C. Brune, Nucl. Phys. A 596 (1996) 122.

[35] R.B. Wiringa, V.G.J. Stoks, R. Schiavilla, Phys. Rev. C 51 (2001) 38.

[36] M. Schmidt, G. Röpke, H. Schulz Ann. Phys. (N.Y.) 202 (1990) 57.

[37] S.M. Johns, P.J. Ellis, J.M. Lattimer, Ap. J. 473 (1996) 1020.

[38] M. Abromowitz, I.S. Stegun, *Handbook of Mathematical Functions*, Dover, New York, 1965.

[39] X. Roca-Maza, X. Vinas, M. Centelles, P. Ring, P. Schuck, Phys. Rev. C 84 (2011) 054309.

[40] T. E. O. Ericson, W. Weise, *Pions and Nuclei*, Oxford University Press, Clarendon, Oxford 1988

[41] C. R. Howell et al., Phys. Lett. B 444 (1998) 252.

[42] R. Bryan, B. L. Scott Phys. Rev. 177 (1969) 1435.

[43] T.D. Lee, C.N. Yang, Phys. Rev. 105 (1957) 1119.

[44] J.E. Drut, T.A. Lähde, G. Wlazłowski, P. Magierski, Phys. Rev. A 85 (2012) 051601(R).

[45] J. Carlson, S.-Y. Chang, V.R. Pandharipande, K.E. Schmidt, Phys. Rev. Lett. 91 (2003) 050401.

[46] G. Shen, private communication.